Evaluation of fluorophores to label SNAP-tag fused proteins for multicolor single molecule tracking microscopy in live cells

Peter J. Bosch[1], Ivan R. Corrêa Jr.[2], Michael H. Sonntag[3], Jenny Ibach[4], Luc Brunsveld[3], Johannes S. Kanger[1], Vinod Subramaniam[1, 5,*]

1. Nanobiophysics, MESA+ Institute for Nanotechnology and MIRA Institute for Biomedical Technology and Technical Medicine, University of Twente, Enschede, The Netherlands
2. New England Biolabs, Ipswich, MA, USA
3. Laboratory of Chemical Biology, Department of Biomedical Engineering, and Institute of Complex Molecular Systems, Eindhoven University of Technology, Eindhoven, The Netherlands
4. Max Planck Institute of Molecular Physiology, Dortmund, Germany
5. Present address: FOM Institute AMOLF, Science Park 104, 1098 XG Amsterdam, The Netherlands

[*]Correspondence: subramaniam@amolf.nl

Keywords

Single molecule tracking, multicolor tracking, SNAP-tag, protein mobility, protein interactions, cells, fluorophores

Running title: SNAP-tag probes for live cell microscopy

0

Abstract

Single molecule tracking has become a widely used technique to study protein dynamics and their organization in the complex environment of the cell. In particular, the spatiotemporal distribution of membrane receptors is an active field of study due to its putative role in the regulation of signal transduction. The SNAP-tag is an intrinsically monovalent and highly specific genetic tag for attaching a fluorescent label to a protein of interest. Little information is currently available on the choice of optimal fluorescent dyes for single molecule microscopy utilizing the SNAP-tag labeling system.

We surveyed 6 green and 16 red excitable dyes for their suitability in single molecule microscopy of SNAP-tag fusion proteins in live cells. We determined the nonspecific binding levels and the photostability of these dye conjugates when bound to a SNAP-tag fused membrane protein in live cells. We found that only a limited subset of the dyes tested is suitable for single molecule tracking microscopy.

The results show that a careful choice of the dye to conjugate to the SNAP-substrate to label SNAP-tag fusion proteins is very important, as many dyes either suffer from rapid photobleaching or high nonspecific staining. These characteristics appear to be unpredictable beforehand, which motivated the need to perform the systematic survey presented here. We have developed a protocol for evaluating the best dyes, and for the conditions that we evaluated, we find that Dy 549 and CF 640 are the best choices tested for single molecule tracking. Using an optimal dye pair, we also demonstrate the possibility of dual-color single molecule imaging of SNAP-tag fusion proteins. This survey provides an overview of the photophysical and imaging properties of a range of SNAP-tag fluorescent substrates, enabling the selection of optimal dyes and conditions for single molecule imaging of SNAP-tagged fusion proteins in eukaryotic cell lines.

1

Introduction

Single molecule fluorescence microscopy has emerged in recent years as a powerful tool to investigate the structural dynamics and biological functions of proteins and macromolecular protein complexes (1–5). Single molecule fluorescence approaches can reveal the dynamic interactions of individual proteins and heterogeneity in the spatial distribution of proteins that are difficult to detect using other fluorescence microscopy approaches (6–8). Despite the extraordinary advances in single molecule fluorescence achieved to date, there remain many technical challenges that must be overcome to systematically study proteins in their native highly complex cellular environment. One of the challenges involves the specific and monovalent labeling of proteins of interest with a photostable fluorescent probe. In the last decade several technologies have been developed that permit proteins to be specifically tagged with organic dyes in live cells (2, 3, 9–11). In this paper we focus on the fluorescent labeling of proteins for single molecule tracking.

Single molecule fluorescence microscopy allows the tracking of proteins in a living cell at high resolution for a short period of time (12–15). The trajectories obtained contain valuable spatiotemporal information on interactions of proteins with their microenvironment (16–18). For instance, a protein may interact with other molecules resulting in transient slowed diffusion or confinement by the cytoskeletal or other nanoscale compartmentalization structures in the plasma membrane (11, 15, 19–23). One of the main advantages of single molecule fluorescence microscopy is the ability to track single protein molecules to provide details on the kinetics of protein association and dissociation. When the trajectories of a single protein species are recorded in multiple colors, they can reveal the kinetics of homo-dimerization interactions by co-movement of the labeled molecules (11, 24). For this co-movement analysis, the protein species needs to be labeled with fluorophores emitting light at spectrally distinct wavelengths to allow simultaneous visualization at high resolution of two distinct proteins (of one protein species). Knowledge of protein interactions and their kinetics is important to understand the underlying signal transduction mechanisms and to model the cellular signal regulatory system (25–27).

A common approach to fluorescently label proteins is by cloning and expressing the protein of interest fused to an autofluorescent protein (FP). Several FPs are currently available that are suitable for single molecule tracking, such as mCitrine, mCherry (28), and the infra-red iRFP (29). While these genetically encoded labels allow multi-color tracking, FPs cannot match the photostability of small organic dyes (2, 30), limiting the timescale over which a protein can be tracked, and the accuracy with which it can be localized. To permit imaging of longer trajectories, fluorescent probes should ideally be bright and photostable (i.e. slow to photobleach) in addition to being specifically linkable to the protein of interest. The tools of choice in this case are organic dyes and quantum dots (Qdots). Although Qdots are extremely bright and photostable, they are larger than most proteins themselves, which might sterically hinder the movement of the protein (31). Additionally, the use of monovalent quantum dots requires custom fabrication (32–34), and they might suffer from nonspecific labeling or aggregation (35, 36).

2

More recent genetic techniques allow the specific and monovalent labeling of recombinant proteins with small organic fluorophores in live cells. Labeling by means of protein tags complements other approaches to label proteins with organic fluorophores such as labeling with fluorescently labeled ligands and immunostaining with antibodies or Fab fragments. Since the tag does not compete with ligand binding and has no antagonistic function, the effects of ligands or inhibitors on ligand-free and fully functional receptors can be studied. The monovalency of the substrates ensures that no artificial clustering is induced. Among the most versatile of the protein tags is the SNAP-tag, a 20 kDa mutant of the human DNA repair protein O^6-alkylguanine-DNA alkyltransferase (hAGT) that reacts specifically and rapidly with benzylguanine (BG) or benzylchloropyrimidine (CP) derivatives, leading to a covalent labeling of the SNAP-tag with a synthetic probe (37–41). The reaction occurs through a well-defined mechanism and predictable monovalent stoichiometry. For example, BG substrates derived from organic fluorophores react with SNAP-tag to provide specific labeling of a protein species with a fluorescent label at physiologically relevant conditions in the cell (Fig. 1). For labeling at the single molecule level, SNAP-tag is especially suitable to label plasma membrane resident proteins using membrane impermeable substrates.

There is a wide variety of reported applications in protein labeling for the SNAP-tag system, including super-resolution imaging (42–44), analysis of protein function (45) and protein half-life (46), protein-protein interactions (47), sensing cell metabolites (48), and for the identification of drug targets (49). SNAP-tag labeling has also been utilized to study several protein complexes at the single molecule level (50–59). Although the application of the SNAP-tag labeling system for single molecule tracking had already been suggested (14), only recently have Calebiro et al. demonstrated the first example (to the best of our knowledge) of this tagging technology for single color fluorescence tracking (60). These authors used direct receptor labeling with SNAP-tag to dynamically monitor the adrenergic receptors β1AR and β2AR and the γ-aminobutyric acid GABAB receptor on intact cells, and compared their spatial arrangement, mobility, and supramolecular organization. Benke et al. have recently shown a new approach to single molecule tracking by using the blinking properties of synthetic dyes attached to SNAP-tag (61). While this approach optimizes the total number of observable diffusion steps, it does not facilitate the observation of a single protein for as extended a period of time as possible, a requirement to study binding associations.

Here we report a comprehensive survey on the photostability and binding specificity of several SNAP-tag fluorescent substrates using widefield and total internal reflection fluorescence (TIRF) single molecule microscopy. We have investigated the suitability of 22 fluorescent substrates (BG-dyes) by characterizing their properties in living cells using a C-terminal (extracellular) SNAP-tag fusion to the epidermal growth factor receptor (EGFR), a plasma membrane resident protein. Due to the significant autofluorescence of cells when using blue excitable dyes, we limited our survey to green- and red-excitable dyes. Since a lot of dyes are available in this spectral range, we selected dyes from different manufacturers which are commonly available and used, and tried to include dyes from various chromophore families. We emphasize that it is essential to study the fluorophores in the cellular setting, because photophysical properties are known to differ depending on the nature of their

conjugate and its microenvironment. For example, different photostabilities have been observed for fluorescent proteins on different interfaces, due to the apparent role of the protein shell rigidity for each chromophore (62). In addition, the fluorescence of a number of fluorophores may be quenched by electron donors like guanine, tryptophan, etc. (63). Therefore the photophysical properties of free substrates in solution or immobilized on a glass surface do not necessarily reflect their properties after reaction with the SNAP-tag fused protein. Very recently, the photostability of two red-excitable fluorescent substrates was measured for another protein tag (A-TMP) at the single molecule level (64). The binding specificity for these substrates was not determined.

Methods

Chemicals, Purification and Analysis of SNAP-tag Substrates
Commercially available compounds were used without further purification. SNAP-Surface Alexa Fluor 546 (BG-Alexa 546), SNAP-Surface 549 (BG-Dy 549), SNAP-Surface 632 (BG-Dy 632), SNAP-Surface 647 (BG-Dy 647), SNAP-Surface Alexa Fluor 647 (BG-Alexa 647), SNAP-Surface 649 (BG-Dy 649) were obtained from New England Biolabs, Inc.

BG-Atto 550, BG-Atto 565, BG-Atto 620, BG-Atto 633, BG-Atto 647N, BG-Atto 655, and BG-TF5 have been described previously (40–42, 65). The remaining substrates for the labeling of SNAP-tag fusion proteins were prepared by reacting the building block BG-NH$_2$ (S9148, New England Biolabs, Inc.) with commercially available *N*-hydroxysuccinimide esters (NHS) of the corresponding fluorophores. Atto Rho6G and Atto 532 were obtained from Atto-Tec GmbH (Siegen, Germany); Dy 549, Dy 630, Dy 634, Dy 648, and Dy 651 were obtained from Dyomics GmbH (Jena, Germany). CF633 and CF640R were obtained from Biotium Inc. (Hayward, CA, USA), and Star635 was obtained from Abberior GmbH (Göttingen, Germany).

BG-549-549, BG-Dy 651, BG-CF 633, BG-CF 640R, and BG-Star 635 were purified and analyzed with the following equipment. Reversed-phase high-performance liquid chromatography (HPLC) was performed on Agilent LC/MS Single Quad System 1200 Series (analytical) and Agilent 1100 Preparative-scale Purification System (semi-preparative). Analytical HPLC was performed on Waters Atlantis T3 C18 column (2.1 x 150 mm, 5 µm particle size) at a flow rate of 0.5 mL/min with a binary gradient from Phase A (0.1 M triethyl ammonium bicarbonate (TEAB) or 0.1% trifluoroacetic acid (TFA) in water) to Phase B (acetonitrile) and monitored by absorbance at 280 nm. Semi-preparative HPLC was performed on VYDAC 218TP series C18 polymeric reversed-phase column (22 x 250 mm, 10 µm particle size) at a flow rate of 20 mL/min. Mass spectra were recorded by electrospray ionization (ESI) on an Agilent 6120 Quadrupole LC/MS system. BG-Atto Rho6G, BG-Dy 630, BG-Dy 634, and BG-Dy 648 were purified and analyzed with the following equipment. Reversed-phase high-performance liquid chromatography (HPLC) was performed on Shimadzu SCL-10 AD VP series (analytical) and Shimadzu LC-20 AD System (preparative). Analytical HPLC was performed on a reversed phase HPLC column (GraceSmart PP18, 50 mm x 2.1 mm, 3µm) at a flow rate of 0.20 mL/min and a binary gradient of acetonitrile in

4

water (both containing 0.1% formic acid) at 298K. Mass and UV-VIS spectra were recorded with an Ion-Trap (LCQ Fleet Ion Trap Mass Spectrometer, Thermo Scientific) and diode array detector (Finnigan Surveyor PDA Plus detector, Thermo Electron Corporation). Preparative reversed-phase HPLC was performed on a reversed phase HPLC column (GraceAlpha C18 5u, 250 mm x 4.6 mm) at a flow rate of 1 mL/min with an isocratic gradient of Phase A (0.1 % formic acid in water or 25 mM ammonium acetate in water, pH 4) to Phase B (0.1 % formic acid in acetonitrile) and monitored with a UV-VIS detector (SPD-10AV VP series, Shimadzu).

Further details of the synthesis of the SNAP-tag substrates are described in the Supporting Material.

Cell culture

All cell culture materials were obtained from PAA Laboratories (Pasching, Austria) unless stated otherwise. The MCF7 epithelial human breast cancer cell line was bought from ATCC. MCF7 cells were cultured in high glucose Dulbecco's Modified Eagle's medium (DMEM) supplemented with 10% FBS and Pen Strep at 37°C with 5% CO_2. The H441 epithelial human lung adenocarcinoma cancer cell line was a gift from Anton Terwisscha van Scheltinga (Department of Medical Oncology, University of Groningen, The Netherlands). These cells were cultured in Roswell Park Memorial Institute (RPMI) 1640 medium supplemented as above. The HeLa epithelial human cervix adenocarcinoma cancer cell line was a gift from Wilma Petersen (University of Twente, The Netherlands), and was cultured in Iscove's Modified Dulbecco's Media (IMDM) supplemented as above.

The SNAP-EGFR construct was cloned as detailed in the Supporting Material. We created stably expressing SNAP-EGFR HeLa cells by transfecting HeLa cells in a 60 cm^2 well of 40%-confluent cells using 9 µg of SNAP-EGFR plasmid DNA and 20 µL Lipofectamine LTX and 9 µL Plus reagent (Invitrogen) in 15 mL Pen Strep free cell medium, as described in the suppliers' protocol. Selection (1400 µg/mL of active G418) was applied after 24 h. After 5 days the cells were split over two 6-well plates. After 10 days the wells were screened for expression of SNAP-EGFR by labeling with 500 nM BG-Alexa 546 for 15 min and fluorescence microscopy analysis on the single molecule sensitive microscope as described later. Note that the expression level can be very low at this stage, and the imaging required a single molecule sensitive fluorescence microscope. One well contained positive cells with an expression level slightly above the single molecule level; these cells were further cultured. For culturing, the concentration of active G418 was 350 µg/mL.

Sample Preparation

For each dye, video recordings were taken of four samples: the SNAP-tag positive cells and the three negative cell lines. Before measurements, HeLa cells stably expressing SNAP-EGFR, HeLa cells, MCF7 cells, and H441 cells were plated in Greiner Bio CellView dishes (product #627870) in full medium, and left overnight to allow the cells to adhere to the glass. The HeLa cells stably expressing SNAP-EGFR were also starved in FBS free medium and left for another night to reduce the activity and internalization of the EGFR fusion protein. On the day of the experiment, cells were washed with starvation medium containing 0.5% BSA.

5

Labeling of the SNAP-EGFR proteins was carried out thereafter by incubating the cells for 2 minutes (± 10 seconds) with 400 nM of each BG-dye in starvation medium containing 0.5% BSA. Samples were washed immediately by replacing the labeling solution with PBS buffer supplemented with magnesium and calcium. This washing step was repeated at least three times. Incubation and washing of the SNAP-tag negative cells with the substrates was performed using the same conditions.

Microscopy settings

The microscope hardware is described in the Supporting Material. Measurements to determine nonspecific binding of the SNAP substrates were performed using widefield and TIRF illumination. Measurements to determine the photobleaching of the substrates were performed using widefield illumination. The illumination time differed for each fluorescent substrate, and was chosen in such a way that single molecules were clearly visible over the autofluorescence background of the cell. We sought to collect the same average number of photons per molecule in a frame for each fluorescent substrate. Since the quantum yield has not been previously determined for all fluorescent substrates, the illumination time to yield an equal number of emitted photons per molecule could not be calculated beforehand. Videos were recorded at 20-30 fps, which is the highest allowed frame rate of the camera at the maximum readout rate of 10 MHz and frame size of 512x512 pixels. Each video recording consisted of 800 frames. Before recording each video, a minimal number of frames (approximately 10 to 30 frames) were used to focus on the basal membrane of the cell.

Single molecule brightness

To allow conversion of pixel counts to photons, a calibration of the gain of the two EMCCD cameras was performed by the mean-variance method (Fig. S1). The slope of the line in this curve is equal to the inverse gain of the camera. A gain of 49.9 ± 0.1 was found for the camera recording the green-excitable dyes, and a gain of 32.5 ± 0.1 was found for the camera recording the red-excitable dyes. The pixel intensities in counts are divided by the camera gain to convert the pixel intensities to photons. The brightness of one molecule (sometimes also termed spot intensity) was calculated as the integrated intensity of a single molecule using a Gaussian fit performed by the tracking algorithm used (66). This yields for all single molecules the number of detected photons per single molecule per frame. We defined the single molecule brightness B as the average of these numbers in one recording.

The brightness of the dye conjugates can be compared between dyes by a relative brightness (Table S1), which is a normalized value given by the single molecule brightness B (Fig. S2) divided by the acquisition time, the excitation efficiency η_e, the emission efficiency, and by the laser excitation power. The excitation efficiency η_e is equal to the fraction of the maximum value of the excitation spectrum of the dye at the wavelength of the lasers, i.e. 532 nm for the green dyes, and 637 nm for the red dyes. The spectra of the dyes were downloaded from the SemRock website (http://www.semrock.com), except for the CF dyes, TF5 and Star635; we measured the spectra for these dyes with a Varian Cary Eclipse fluorescence spectrophotometer (Palo Alto, CA).

6

Tracking of single molecules

To obtain trajectories from the raw videos, we used previously described tracking software (11, 66). The settings used for the cost matrices in this software can be found in the supplementary information. For the initial detection of molecules the tracking algorithm uses an intensity threshold. This threshold was taken the same for all video series of one fluorescent substrate to obtain a fair comparison of the level of specific and nonspecific labeling. The threshold was determined in the situation where the substrates are incubated with SNAP-tag expressing cells (specifically attached); we used the same threshold values in the detection of nonspecifically attached substrates.

After obtaining the single molecule trajectories, two filtering operations were applied with the purpose of discarding very short tracks, and differentiating between completely immobile and (transiently) mobile molecules. Very short tracks (having less than 7 localizations in total) were excluded as they did not contain much significant information; there is also a higher chance that a fluorescent spot that is detected only for a few frames was attributable to noise rather than to a specifically labeled fluorescent molecule. A segment of a track was defined as the subsequent positions of a fluorescent molecule in adjacent frames. This meant that blinking of a dye resulted in multiple segments within a track. Immobile tracks were discarded because they often represented dye molecules bound to the glass surface, and were detected using a radius of gyration algorithm (67). The threshold for the trajectory area was defined by a gyration radius of 40 nm, as this corresponded to the apparent area travelled by an immobile molecule due to the localization accuracy.

Analysis of single molecule photobleaching rate

The number of fluorescent molecules $N(i)$ in each frame i was determined for each recording. Since photobleaching follows an exponential decay profile, the photobleaching rates are obtained for each video recording by fitting the number of molecules over time with a one component exponential function without offset:

$$N(i) = N(1) \cdot \exp(-1/\tau \cdot i) \tag{1}$$

where i is the framenumber, τ is the mean photobleaching time (in frames), hence $1/\tau$ is the rate of photobleaching per frame, and $N(1)$ the fitted number of molecules in this first frame ($i=1$). The fit was performed over framenumbers 20 till 600. In the first few frames the autofluorescence of the cells might obscure a proper detection of single molecules by the algorithm. Because the autofluorescence bleaches rapidly, the fluorescent molecules can be reliably detected after 20 frames. At frame 600 the number of molecules were reduced to a basal level in most recordings. The fluorophore's mean photobleaching time τ is multiplied by the single molecule brightness B. This yields the expected average number of detected photons per molecule P.

Since the dye conjugates have different emission spectra, we corrected for the transmission efficiency of the filter set to obtain a precise comparison of the dyes. The most relevant parameter to compare is the photobleaching rate per *emitted* photon and not per *detected*

7

photon. This is because not all the emitted photons pass the filters placed before the camera. Not all the emitted photons are collected by the objective, but the fraction of photons collected is the same for all the dyes, and it is therefore not necessary to correct for this. Furthermore the quantum efficiency of the CCD chip is similar around the measured wavelengths. Therefore the photobleaching rates were only corrected for the efficiency of the filter set η_f, which describes the efficiency with which the emitted fluorescence passed the filter set used. The expected number of detectable photons P_{corr} is given by the expected *detected* number of photons P divided by the detection efficiency η_f. The detection efficiency η_f of a dye was determined by integration over the combined transmission spectrum of the dichroic mirrors and the emission filter multiplied by the normalized emission spectrum of the dye. This efficiency is listed for each dye in Table S1 in the Supporting Material. The expected number of detectable photons per molecule P_{corr} was calculated as:

$$P_{corr} = \frac{1}{\eta_f} \cdot B \cdot \tau \qquad (2)$$

Results

Nonspecific binding of the SNAP substrates

We first screened the dyes to assess the level of nonspecific staining of the dye conjugates in cells not expressing the SNAP-tag fusion protein (SNAP-tag negative cells). We excluded substrates leading to high nonspecific staining of intracellular structures from further analyses. The results from microscopy video recordings of H441 cells incubated with each dye conjugate are shown in Fig. 2 (widefield illumination), and in Fig. S3 (TIRF illumination). In all the images there was full confluence of cells in the field of view. While TIRF images are often preferred over widefield images to record receptor proteins due to the reduced background level, likewise, only nonspecific staining near and at the plasma membrane of the cells will be observed with TIRF imaging. Nonspecifically stained intracellular structures were better observed using widefield imaging, and were used for screening of nonspecific staining. The screening for nonspecific binding was based on observations of at least 50 cells per sample, and resulted in the exclusion of the following substrates: Atto-550, Atto-565 Atto-620, Atto-633, Atto-647N, Dy-630, Dy-651, and Star-635.

The fluorescent substrates tested exhibited similar levels of nonspecific staining in HeLa cells (data not shown). The nonspecific staining observed did not appear to substantially vary among cells in the same sample, or between the same samples prepared on different days. Dead cells usually showed much more nonspecific staining than healthy cells.

The remaining dye conjugates were incubated with SNAP-tag negative HeLa, MCF7 and H441 cells. Microscopy recordings were taken for each SNAP substrate in the different cell lines, with the focus of the microscope at the basal membrane of the cells. The tracking algorithm provided the number of detected molecules in each frame. For each substrate the

8

camera acquisition time used was the same as that used in the recordings with the SNAP-tag positive cells, see Table S1. This ensured that the number of detectable nonspecific molecules was determined under the same imaging and tracking conditions as for the imaging of specifically bound molecules. Next we differentiated completely immobile molecules from (transiently) mobile molecules. Completely immobile molecules are often molecules bound to the glass substrate; these are typically of less concern, since they can usually be readily excluded before further analysis. In contrast, nonspecific mobile molecules obscure the analysis of the specifically labeled protein molecules.

The average number of mobile molecules as well as the total number of molecules (mobile and immobile) detected in frame numbers 20-40 are shown in Fig. 3. The first 20 frames were excluded because the autofluorescence of the cells is then particularly high, which obscures the specific detection of labeled proteins. Only regions with full confluence of cells were recorded. The total number of nonspecific molecules per field of view is a measure of the expected number of molecules adsorbed on the glass substrate (underneath the cells), the immobile molecules, plus the number of false positive molecules on the plasma membrane, the (transiently) mobile molecules. The number of nonspecific molecules in frame numbers 120-140 is also shown to get insight in the photobleaching of nonspecifically bound substrates.

Photostability of the substrates bound to SNAP-tag
To determine the photostability of the dyes bound to SNAP-tag, we incubated them with cells expressing the SNAP-EGFR fusion protein. Microscopy recordings were taken for each dye conjugate to determine the photobleaching rate of the dyes bound to SNAP-tag. A stably transfected HeLa cell line, which had low expression levels of SNAP-EGFR (single molecule density), was utilized to avoid variance between cells of different samples as a result of transfection. We optimized the incubation concentration and time for high labeling efficiency and low nonspecific binding using a titration series with BG-Alexa 546, and found that 2 minutes with 400 nM of substrate were enough for a complete labeling with this dye (and also used these incubation conditions in the nonspecific binding assay). Note that incubation using elevated dye concentrations or prolonged incubation time might result in higher nonspecific binding levels. For each dye conjugate, we observed a similar percentage of labeled cells (estimated to be 15%) irrespective of the specific dye choice. We believe that this percentage of labeled cells was caused by a large population of cells that do not express the SNAP-tag. The fraction of SNAP-tag receptors labeled in cells appeared to vary slightly from dye to dye.

For an accurate comparison, we aimed to obtain the same number of detected photons per frame (single molecule brightness B) for all green and all red dyes. All the dyes were bright enough to be detected at a single molecule level in a widefield setup in the presence of cellular autofluorescence background. A widefield setup is more appropriate than a TIRF setup for an accurate comparison as the single molecule brightness B is very difficult to control in TIRF due to varying TIRF angles and the presence of molecules at different depths. Furthermore, the expected number of photons emitted from a fluorophore does not depend on the type of illumination. For the characterization procedure followed, we found that an optimal single molecule brightness was $B = 150$ photons for red excitable dyes and $B = 200$

9

photons for green excitable dyes. Some dyes needed a relatively long acquisition time to obtain the targeted single molecule brightness B (see Table S1 for the acquisition times used and Fig. S2 for the resulting single molecule brightness B). Table S1 also lists the relative brightness of each dye conjugate to SNAP-tag. At least four videos of different cells were recorded and analyzed per dye conjugate (Fig. 4A and Video 1). The brightness (spot intensity) of the molecules follows a Poisson like distribution, as shown in Fig. 4B.

Due to photobleaching, the number of observed fluorescent molecules $N(i)$ decreased over time (Fig. 4C). We fitted the rate of photobleaching using Eq. 1 to extract the mean photobleaching time τ for each fluorophore. Using Eq. 2 the expected number of detectable photons per molecule P_{corr} was calculated. A basal level of detected molecules was observed even after a long imaging time. We believe that these remaining molecules are the result of molecules in an intermittent state (blinking) and a constant influx of molecules from out-of-focus areas into focus. The expected number of detectable photons per molecule P_{corr} was obtained from multiple recordings per fluorescent substrate, and the average value and standard deviation are shown in Fig. 5. The conversion from numbers of molecules to photons requires that single molecules are detected. This was checked by confirming that the number of emitted photons per molecule does not vary over time (Fig. 4D).

In Fig. 6 we summarize the results for nonspecific binding versus the photostability for each dye. From this figure it is clear that both green (e.g. Dy 549) and red excitable dyes (e.g. CF633 and CF640) are suitable for single molecule tracking. This result allowed us to examine the possibility to simultaneously label the SNAP-tag with two spectrally different dyes. The simultaneous incubation of a 1.0:0.67 mixture of BG-CF633 and BG-Dy 549 resulted in roughly equal labeling of the SNAP-tag receptor with these two dyes (Fig. 7). Video 2 shows SNAP-EGFR proteins labeled with these two dyes diffusing in the plasma membrane of a live cell. The disappearing of receptors is due to photobleaching.

Discussion

The results show that a careful choice of the dye to conjugate to the SNAP-substrate to label SNAP-tag fusion proteins is very important, as many fluorescent substrates either suffer from rapid photobleaching or high nonspecific staining. We found that three fluorescent substrates out of the 22 substrates tested can be used for single molecule tracking applications as these substrates combine both a low level of nonspecific binding and a high photostability. Among the green-excitable fluorescent substrates, BG-Dy 549 showed the highest photostability with the lowest nonspecific staining (Fig. 6). As an alternative, BG-Alexa 546 could be used in ensemble measurements (e.g. FRET studies), as it is photostable and only results in detectable nonspecific binding at the single molecule level. Among the red-excitable fluorescent substrates, BG-CF640 and BG-CF633 exhibited the best results (Fig. 6). Whereas BG-CF640 showed slightly lower nonspecific staining, CF633 might be relatively brighter depending on the filter sets available. Even though BG-Atto 655 showed the highest photostability among the substrates tested (Fig. 5), its use is limited to ensemble measurements, since it showed high levels of nonspecific binding to membrane components of all the three cell lines (Fig. 3).

10

Nonspecific binding of the SNAP substrates

One of the main advantages of single molecule tracking techniques is the ability to discriminate single mobile molecules from cellular autofluorescence, immobile fluorescent molecules, and clusters of fluorescent molecules. We utilized this to characterize the nonspecific binding of the fluorescent substrates. Dealing with the nonspecific binding of fluorophores to any cellular components is one of the biggest challenges in microscopy. Several of the BG-dyes tested showed high levels of nonspecific binding (Fig. 2). We found that the amount of nonspecific binding of the BG-dyes is roughly the same among the cell lines tested (Fig. 3). None of the dyes that led to appreciable levels of nonspecific staining photobleached within a short period (Fig. 3); hence differences in photobleaching of specifically and nonspecifically bound dyes cannot be used advantageously to discriminate between the two cases.

The cause of nonspecific binding might be explained from a molecular perspective. Several dyes contain long chain hydrocarbons which are lipophilic; therefore they easily incorporate in lipid rich structures such as cellular membranes. Sulfonate acid groups are often added to dyes to enhance their solubility in water. These groups are negatively charged and electrostatically repelled away from the negatively charged lipid headgroups in cellular membranes. Negatively charged dyes include sulfonated fluorescein- and cyanine-based dyes (68). On the other hand, cationic (positively charged) dyes, such as many rhodamine based dyes have been reported to bind to mitochondria in live cells (69). Therefore, the major factors influencing nonspecific binding might be the lipophilic character of a dye in combination with localized electronic charges. Furthermore, the inability of certain dyes to penetrate the plasma membrane hinders access to intracellular structures. In general, neutral and anionic (negatively charged) dyes in this survey appeared to have less tendency to bind to cellular substructures (e.g., Alexa 546/647, Dy 632/634, Dy 648/649). Some dyes (e.g., Atto 647N, Dy 651) adhered in a large extent to the glass coverslip (and may perhaps be avoided by optimizing cleaning procedures), obscuring the detection of specifically bound single molecules in the adjacent plasma membrane of the cell. The complex effects of local charges in combination with polar and lipophilic groups in a dye molecule make it difficult to predict the nonspecific binding ability of dyes beforehand. For example, the net charge of a molecule does not completely explain the nonspecific interaction, such as for the negatively charged BG-Dy 651 and the neutrally charged BG-Dy 630. Both showed a considerable amount of nonspecific binding to cellular components. We also did not find a correlation between the chromophore family and the nonspecific labeling level. For example, the incubation of cells with the rhodamine derived dyes BG-Alexa 546 and BG-Atto 532 resulted in low nonspecific levels, while BG-Atto 550 and BG-Atto 565 led to much higher nonspecific levels. Likewise the cyanine based BG-Alexa 647 showed almost no nonspecific binding, while the BG-Dy 630 exhibited extremely high nonspecific binding.

Benke et al. have reported the use of five BG dyes for single molecule tracking in eukaryotic cells (61). In their approach, the fluorescence of these dyes was stochastically activated for super-resolution microscopy; however, no data on nonspecific binding was provided. Stöhr et al. described the quenching of several dyes after conjugation to BG and subsequent SNAP-tag

11

binding (63, 70). Their data demonstrates that the photophysics (i.e. the photobleaching time and fluorescence quenching) of a given dye can be altered by its molecular environment. Furthermore they conclude that it is impossible to predict the changes in fluorescence beforehand due to the complex effects of local charges in the dye molecule. Stöhr et al. also reported on the background levels of remaining unreacted dyes inside *E. coli* after washing protocols. Interestingly, some substrates such as BG-Atto 620 and BG-Atto 633, which reportedly exhibited a low background staining in *E. coli*, led to a surprisingly high nonspecific binding in our experiments with mammalian cell lines. Stöhr et al. also reported the labeling of 3T3 fibroblast cells with BG-Atto 550, BG-Atto 633 and BG-Atto 647N. Similarly, we noticed that BG-Atto 550 and BG-Atto 647N produced high levels of nonspecific binding. However, in contrast to Stöhr et al., in our hands BG-Atto 633 showed a very intense nonspecific staining of cytosolic and membrane structures (Fig. 2 and Fig. S2). This discrepancy could be caused by the different fluorescence intensity levels in both studies, as we looked at nonspecific staining in the context of single molecules.

Photostability of the substrates bound to SNAP-tag
Whereas many red-excitable dye conjugates did not show any substantial nonspecific binding levels, these dyes appeared to be less photostable than the green-excitable dyes. Two dyes (CF633 and CF640) are photostable enough to permit prolonged imaging with low nonspecific staining (Fig. 6). Between these two dyes, CF640 showed marginally less nonspecific staining (Fig. 3).

Another noteworthy observation was that the photostabilities of the Dy dyes of relatively close excitation wavelengths were very similar (Fig. 5), for instance Dy 647, 648 and 649, and also Dy 632 and 634. From a molecular perspective, Dy 647, 648, and 649 are typical cyanine dyes, while Dy 632 and 634 have one indole group with a polymethine chain linked to a benzopyrylium group. The slight differences in these chromophores did not seem to have a large effect on its photobleaching rate.

Complications and validity
We have performed the photobleaching experiments on SNAP-tag fused transmembrane EGFR proteins, which have a basal internalization rate even when the cells are starved (71, 72). This might lead to a false enhanced bleaching detection. During the 30 seconds of imaging, however, the internalisation rate of the receptor is small compared to the photobleaching rate (73). Even one hour after the labeling, no significant decrease of receptor molecules was observed at the plasma membrane of the cells. However, in some instances a small increase in fluorescence in the cytosol was noticeable, which could be an attributed to the basal level of receptor internalization and the recycling process. Another complication stems from the fact that this receptor seems to localize more in filopodia and the periphery of the cells (74); these receptors can diffuse more easily in and out of focus. Because molecules diffusing in and out of the plane of focus will likely be in equilibrium, this should not influence the recorded bleaching rate at the beginning of a recording when receptors in focus have not been bleached yet. Later, however, while bleached receptors leave the plane, unbleached receptors can enter the focal plane from outside the plane, causing a slower bleaching rate than the actual rate. Therefore, we derived the bleaching rate from that part of

the recordings where the number of molecules is still decreasing. Furthermore, the rate of receptors entering the focal plane within the 30 seconds of imaging will be limited, and this rate will be independent of the dye used.

Improvements to fluorescent SNAP substrates

The attachment of two Dy 549 dyes on a single SNAP substrate (Dy 549x2) seems an interesting approach to prolong imaging of the protein, as its photostability almost doubled compared to the substrate with single loaded Dy 549 (Fig. 5). The brightness of the double loaded SNAP substrate was similar to the single loaded substrate (Table S1). This might be due to self-quenching, which is commonly observed when increasing the number of fluorophores on a protein, and affects the fluorescence intensity but not the photobleaching rate per photon for the complex. Further studies are needed to confirm that the (single molecule) brightness is indeed similar in SNAP substrates with one, two, or even more Dy 549 fluorophores.

Another interesting point is the incorporation of a strong fluorescence quencher in the guanine group. Such a fluorogenic method ensures that the benzylguanine coupled fluorophore becomes dramatically more fluorescent upon binding to the SNAP-tag (40). Although the guanine itself already acts as a relatively good quencher for several dyes (63), the more dramatic fluorogenic approach could bypass the issue of nonspecific binding for extremely photostable dyes such as Atto-655. Another interesting idea is to use a SNAP-tag substrate derivatized with a fluorophore and a triplet-state quencher (e.g. a molecular oxygen reducing agent) (75). This strategy has led to an overall decrease of dark state transitions which led to up to 25 fold longer imaging periods (75). Prolonged imaging might allow to observe and follow many more interactions of the protein on its path through the cell.

Conclusions

We have screened and analyzed the photostability and nonspecific binding properties of a wide range of green- and red-excitable dyes for labeling proteins in cells by means of the SNAP-tag technology. The SNAP-tag labeling strategy is particularly useful for labeling proteins on the plasma membrane, since there are no restrictions on the membrane permeability of the fluorescent label. Properties of dyes have generally been determined in ensemble fluorescence imaging and on relatively large biomolecules such as antibodies. However, properties of dyes can be rather different at the single molecule level and when conjugated on a small biomolecule, such as the SNAP substrate (BG), and in the local microenvironment of the SNAP-tag. We have characterized the photostability and specificity for several SNAP-substrate dye conjugates in different cell lines at a single molecule level. We performed the characterization in widefield mode to prevent illumination variations experienced in a TIRF setup, and at high single molecule brightness to adequately count most dye molecules in the recordings. To provide a meaningful comparison, we used similar photon counts per single molecule for each spectrally similar dye, corrected for the detection efficiency of our microscope for the dye's emission spectrum, and performed the tracking of the bound dyes to differentiate the motion of the nonspecifically bound molecules.

13

We found that in our system the SNAP substrates labeled with Dy 549, CF633, and CF 640 are the best choices to label SNAP-tag fusion proteins for single molecule tracking among the fluorescent substrates tested. Also, we have shown that the attachment of two Dy-549 dyes on one BG probe is an interesting approach to prolong imaging of the protein. Finding two spectrally different dyes for labeling SNAP-tag that were suitable for single molecule imaging proved to be a challenge, as most of the fluorescent substrates tested showed either a large amount of nonspecific fluorescence or were rapidly photobleached.

Since both green- and red-excitable fluorescent SNAP substrates have been identified, multi-color single molecule imaging of the same protein species can become a routine experiment by simultaneously incubating these substrates with the SNAP-tag fusion proteins in live cells. This should allow the direct observation of homo-dimers. For an extension to three-color single molecule imaging, BG–Alexa 488 could be used since it is already known to be a suitable dye for single molecule tracking (61), although the intense cellular autofluorescence at this wavelength limits its use to total internal reflection fluorescence (TIRF) microscopy. We anticipate that our conclusions could be extended to the chemically similar tagging technology CLIP-tag, which also has the guanine moiety in its substrate. Our results are probably not directly translatable to chemically different molecular tags, such as Halo, ACP and MCP. The combination of SNAP-tag with another molecular labeling tag allows orthogonal labeling on two different protein species. An interesting extension to one protein species studies is therefore the direct visualization of two interacting proteins of different protein species, such as in heterodimer formation.

Acknowledgement

References

1.   Kusumi, A., C. Nakada, K. Ritchie, K. Murase, K. Suzuki, H. Murakoshi, R.S. Kasai, J. Kondo, and T. Fujiwara. 2005. Paradigm shift of the plasma membrane concept from the two-dimensional continuum fluid to the partitioned fluid: high-speed single-molecule tracking of membrane molecules. Annu. Rev. Biophys. Biomol. Struct. 34: 351–78.

2.   Xia, T., N. Li, and X. Fang. 2013. Single-molecule fluorescence imaging in living cells. Annu. Rev. Phys. Chem. 64: 459–80.

3.   Joo, C., H. Balci, Y. Ishitsuka, C. Buranachai, and T. Ha. 2008. Advances in single-molecule fluorescence methods for molecular biology. Annu. Rev. Biochem. 77: 51–76.

4.   Hinterdorfer, P., and A. van Oijen. 2009. Handbook of Single-Molecule Biophysics. Springer Science+Business Media.

5.   Joo, C., M. Fareh, and V. Narry Kim. 2013. Bringing single-molecule spectroscopy to macromolecular protein complexes. Trends Biochem Sci. 38: 30–37.

6.   Lippincott-Schwartz, J., E. Snapp, and A. Kenworthy. 2001. Studying protein dynamics in living cells. Nat. Rev. Mol. Cell Biol. 2: 444–56.

7.   Miyawaki, A. 2011. Proteins on the move: insights gained from fluorescent protein technologies. Nat. Rev. Mol. Cell Biol. 12: 656–68.

8.   Giepmans, B.N.G., S.R. Adams, M.H. Ellisman, and R.Y. Tsien. 2006. The fluorescent toolbox for assessing protein location and function. Science. 312: 217–24.

9.   Pantoja, R., E.A. Rodriguez, M.I. Dibas, D.A. Dougherty, and H.A. Lester. 2009. Single-Molecule Imaging of a Fluorescent Unnatural Amino Acid Incorporated Into Nicotinic Receptors. Biophys. J. 96: 226–237.

10.   Callegari, A., S. Luin, L. Marchetti, A. Duci, A. Cattaneo, and F. Beltram. 2012. Single particle tracking of acyl carrier protein (ACP)-tagged TrkA receptors in PC12nnr5 cells. J. Neurosci. Methods. 204: 82–86.

11.   Low-Nam, S.T., K.A. Lidke, P.J. Cutler, R.C. Roovers, P.M.P. van Bergen en Henegouwen, B.S. Wilson, and D.S. Lidke. 2011. ErbB1 dimerization is promoted by

domain co-confinement and stabilized by ligand binding. Nat. Struct. Mol. Biol. 18: 1244–1249.

12. Goulian, M., and S.M. Simon. 2000. Tracking single proteins within cells. Biophys. J. 79: 2188–98.

13. Sako, Y., S. Minoghchi, and T. Yanagida. 2000. Single-molecule imaging of EGFR signalling on the surface of living cells. Nat. Cell Biol. 2: 168–72.

14. Wieser, S., and G.J. Schütz. 2008. Tracking single molecules in the live cell plasma membrane-Do's and Don't's. Methods. 46: 131–40.

15. Sergé, A., N. Bertaux, H. Rigneault, and D. Marguet. 2008. Dynamic multiple-target tracing to probe spatiotemporal cartography of cell membranes. Nat. Methods. 5: 687–94.

16. Kholodenko, B.N., J.F. Hancock, and W. Kolch. 2010. Signalling ballet in space and time. Nat. Rev. Mol. Cell Biol. 11: 414–426.

17. Cambi, A., and D.S. Lidke. 2012. Nanoscale membrane organization: where biochemistry meets advanced microscopy. ACS Chem. Biol. 7: 139–49.

18. Saxton, M.J., and K. Jacobson. 1997. Single-particle tracking: applications to membrane dynamics. Annu. Rev. Biophys. Biomol. Struct. 26: 373–99.

19. Kapanidis, A.N., and T. Strick. 2009. Biology, one molecule at a time. Trends Biochem. Sci. 34: 234–43.

20. Schütz, G.J., H. Schindler, and T. Schmidt. 1997. Single-molecule microscopy on model membranes reveals anomalous diffusion. Biophys. J. 73: 1073–80.

21. Brameshuber, M., and G.J. Schütz. 2012. In Vivo Tracking of Single Biomolecules: What Trajectories Tell Us About the Acting Forces. In: Springer Series on Fluorescence. Springer Berlin Heidelberg. pp. 1–37.

22. Dietrich, C., B. Yang, T. Fujiwara, A. Kusumi, and K. Jacobson. 2002. Relationship of lipid rafts to transient confinement zones detected by single particle tracking. Biophys. J. 82: 274–84.

23. De Keijzer, S., A. Sergé, F. van Hemert, P.H.M. Lommerse, G.E.M. Lamers, H.P. Spaink, T. Schmidt, and B.E. Snaar-Jagalska. 2008. A spatially restricted increase in receptor mobility is involved in directional sensing during Dictyostelium discoideum chemotaxis. J. Cell Sci. 121: 1750–7.

24. Cutler, P.J., M.D. Malik, S. Liu, J.M. Byars, D.S. Lidke, and K.A. Lidke. 2013. Multi-color quantum dot tracking using a high-speed hyperspectral line-scanning microscope. PLoS One. 8: e64320.

25. Cebecauer, M., M. Spitaler, A. Sergé, and A.I. Magee. 2010. Signalling complexes and clusters: functional advantages and methodological hurdles. J. Cell Sci. 123: 309–20.

26.   Harding, A.S., and J.F. Hancock. 2008. Using plasma membrane nanoclusters to build better signaling circuits. Trends Cell Biol. 18: 364–371.

27.   Radhakrishnan, K., Á. Halász, M.M. McCabe, J.S. Edwards, and B.S. Wilson. 2012. Mathematical simulation of membrane protein clustering for efficient signal transduction. Ann. Biomed. Eng. 40: 2307–18.

28.   Shaner, N.C., P.A. Steinbach, and R.Y. Tsien. 2005. A guide to choosing fluorescent proteins. Nat. Methods. 2: 905–9.

29.   Filonov, G.S., K.D. Piatkevich, L.-M. Ting, J. Zhang, K. Kim, and V. V Verkhusha. 2011. Bright and stable near-infrared fluorescent protein for in vivo imaging. Nat. Biotechnol. 29: 757–61.

30.   Harms, G.S., L. Cognet, P.H. Lommerse, G.A. Blab, and T. Schmidt. 2001. Autofluorescent proteins in single-molecule research: applications to live cell imaging microscopy. Biophys. J. 80: 2396–408.

31.   Wieser, S., M. Axmann, and G.J. Schütz. 2008. Versatile analysis of single-molecule tracking data by comprehensive testing against Monte Carlo simulations. Biophys. J. 95: 5988–6001.

32.   Howarth, M., W. Liu, S. Puthenveetil, Y. Zheng, L.F. Marshall, M.M. Schmidt, K.D. Wittrup, M.G. Bawendi, and A.Y. Ting. 2008. Monovalent, reduced-size quantum dots for imaging receptors on living cells. Nat. Methods. 5: 397–9.

33.   Liu, H.Y., and X. Gao. 2011. Engineering monovalent quantum dot-antibody bioconjugates with a hybrid gel system. Bioconjug. Chem. 22: 510–7.

34.   Farlow, J., D. Seo, K.E. Broaders, M.J. Taylor, Z.J. Gartner, and Y.-W. Jun. 2013. Formation of targeted monovalent quantum dots by steric exclusion. Nat. Methods. 10: 1203–5.

35.   Pinaud, F.F., X. Michalet, L.A. Bentolila, J.M. Tsay, J.J. Li, S. Doose, G. Sundaresan, A.M. Wu, S.S. Gambhir, and S. Weiss. 2005. Quantum dots for live cells, in vivo imaging, and diagnostics. Science. 307: 538–44.

36.   Pinaud, F., S. Clarke, A. Sittner, and M. Dahan. 2010. Probing cellular events, one quantum dot at a time. Nat. Methods. 7: 275–85.

37.   Keppler, A., S. Gendreizig, T. Gronemeyer, H. Pick, H. Vogel, and K. Johnsson. 2003. A general method for the covalent labeling of fusion proteins with small molecules in vivo. Nat. Biotechnol. 21: 86–9.

38.   Keppler, A., H. Pick, C. Arrivoli, H. Vogel, and K. Johnsson. 2004. Labeling of fusion proteins with synthetic fluorophores in live cells. Proc. Natl. Acad. Sci. U. S. A. 101: 9955–9.

39. Gautier, A., A. Juillerat, C. Heinis, I.R. Corrêa, M. Kindermann, F. Beaufils, and K. Johnsson. 2008. An engineered protein tag for multiprotein labeling in living cells. Chem. Biol. 15: 128–36.

40. Sun, X., A. Zhang, B. Baker, L. Sun, A. Howard, J. Buswell, D. Maurel, A. Masharina, K. Johnsson, C.J. Noren, M.-Q. Xu, and I.R. Corrêa. 2011. Development of SNAP-tag fluorogenic probes for wash-free fluorescence imaging. Chembiochem. 12: 2217–26.

41. Corrêa, I.R., B. Baker, A. Zhang, L. Sun, C.R. Provost, G. Lukinavičius, L. Reymond, K. Johnsson, and M.-Q. Xu. 2013. Substrates for improved live-cell fluorescence labeling of SNAP-tag. Curr. Pharm. Des. 19: 5414–20.

42. Pellett, P.A., X. Sun, T.J. Gould, J.E. Rothman, M.Q. Xu, I.R. Correa Jr., and J. Bewersdorf. 2011. Two-color STED microscopy in living cells. Biomed Opt Express. 2: 2364–2371.

43. Dempsey, G.T., J.C. Vaughan, K.H. Chen, M. Bates, and X. Zhuang. 2011. Evaluation of fluorophores for optimal performance in localization-based super-resolution imaging. Nat. Methods. 8: 1027–36.

44. Klein, T., A. Löschberger, S. Proppert, S. Wolter, S. van de Linde, and M. Sauer. 2011. Live-cell dSTORM with SNAP-tag fusion proteins. Nat. Methods. 8: 7–9.

45. Foraker, A.B., S.M. Camus, T.M. Evans, S.R. Majeed, C.-Y. Chen, S.B. Taner, I.R. Corrêa, S.J. Doxsey, and F.M. Brodsky. 2012. Clathrin promotes centrosome integrity in early mitosis through stabilization of centrosomal ch-TOG. J. Cell Biol. 198: 591–605.

46. Bojkowska, K., F. Santoni de Sio, I. Barde, S. Offner, S. Verp, C. Heinis, K. Johnsson, and D. Trono. 2011. Measuring In Vivo Protein Half-Life. Chem. Biol. 18: 805–815.

47. Ville, D., J. DE Bellescize, M.A. Nguyen, H. Testard, A. Gautier, J. Perrier, M. Till, and V. DES Portes. 2009. Ring 14 chromosome presenting as early-onset isolated partial epilepsy. Dev. Med. Child Neurol. 51: 917–22.

48. Masharina, A., L. Reymond, D. Maurel, K. Umezawa, and K. Johnsson. 2012. A fluorescent sensor for GABA and synthetic GABA(B) receptor ligands. J Am Chem Soc. 134: 19026–19034.

49. Chidley, C., H. Haruki, M.G. Pedersen, E. Muller, and K. Johnsson. 2011. A yeast-based screen reveals that sulfasalazine inhibits tetrahydrobiopterin biosynthesis. Nat. Chem. Biol. 7: 375–83.

50. Hoskins, A.A., L.J. Friedman, S.S. Gallagher, D.J. Crawford, E.G. Anderson, R. Wombacher, N. Ramirez, V.W. Cornish, J. Gelles, and M.J. Moore. 2011. Ordered and dynamic assembly of single spliceosomes. Science. 331: 1289–95.

51. Breitsprecher, D., R. Jaiswal, J.P. Bombardier, C.J. Gould, J. Gelles, and B.L. Goode. 2012. Rocket launcher mechanism of collaborative actin assembly defined by single-molecule imaging. Science. 336: 1164–8.

18

52. Jaiswal, R., D. Breitsprecher, A. Collins, I.R. Correa Jr., M.Q. Xu, and B.L. Goode. 2013. The formin Daam1 and fascin directly collaborate to promote filopodia formation. Curr Biol. 23: 1373–1379.

53. Smith, B.A., K. Daugherty-Clarke, B.L. Goode, and J. Gelles. 2013. Pathway of actin filament branch formation by Arp2/3 complex revealed by single-molecule imaging. Proc Natl Acad Sci U S A. 110: 1285–1290.

54. Smith, B.A., S.B. Padrick, L.K. Doolittle, K. Daugherty-Clarke, I.R. Corrêa, M.-Q. Xu, B.L. Goode, M.K. Rosen, and J. Gelles. 2013. Three-color single molecule imaging shows WASP detachment from Arp2/3 complex triggers actin filament branch formation. Elife. 2: e01008.

55. Peisley, A., M.H. Jo, C. Lin, B. Wu, M. Orme-Johnson, T. Walz, S. Hohng, and S. Hur. 2012. Kinetic mechanism for viral dsRNA length discrimination by MDA5 filaments. Proc. Natl. Acad. Sci. U. S. A. 109: E3340–9.

56. Qiu, W., N.D. Derr, B.S. Goodman, E. Villa, D. Wu, W. Shih, and S.L. Reck-Peterson. 2012. Dynein achieves processive motion using both stochastic and coordinated stepping. Nat. Struct. Mol. Biol. 19: 193–200.

57. Derr, N.D., B.S. Goodman, R. Jungmann, A.E. Leschziner, W.M. Shih, and S.L. Reck-Peterson. 2012. Tug-of-war in motor protein ensembles revealed with a programmable DNA origami scaffold. Science. 338: 662–5.

58. Numata, N., T. Shima, R. Ohkura, T. Kon, and K. Sutoh. 2011. C-sequence of the Dictyostelium cytoplasmic dynein participates in processivity modulation. FEBS Lett. 585: 1185–1190.

59. Yang, Y., and C.Y. Zhang. 2013. Simultaneous Measurement of SUMOylation using SNAP/CLIP-Tag-Mediated Translation at the Single-Molecule Level. Angew Chem Int Ed Engl. 52: 691–694.

60. Calebiro, D., F. Rieken, J. Wagner, T. Sungkaworn, U. Zabel, A. Borzi, E. Cocucci, A. Zurn, and M.J. Lohse. 2013. Single-molecule analysis of fluorescently labeled G-protein-coupled receptors reveals complexes with distinct dynamics and organization. Proc Natl Acad Sci U S A. 110: 743–748.

61. Benke, A., N. Olivier, J. Gunzenhäuser, and S. Manley. 2012. Multicolor single molecule tracking of stochastically active synthetic dyes. Nano Lett. 12: 2619–24.

62. Schenk, A., S. Ivanchenko, C. Röcker, J. Wiedenmann, and G.U. Nienhaus. 2004. Photodynamics of red fluorescent proteins studied by fluorescence correlation spectroscopy. Biophys. J. 86: 384–94.

63. Stöhr, K., D. Siegberg, T. Ehrhard, K. Lymperopoulos, S. Öz, S. Schulmeister, A.C. Pfeifer, J. Bachmann, U. Klingmüller, V. Sourjik, and D.-P. Herten. 2010. Quenched substrates for live-cell labeling of SNAP-tagged fusion proteins with improved fluorescent background. Anal. Chem. 82: 8186–93.

64. Wang, T.Y., L.J. Friedman, J. Gelles, W. Min, A. a Hoskins, and V.W. Cornish. 2014. The covalent trimethoprim chemical tag facilitates single molecule imaging with organic fluorophores. Biophys. J. 106: 272–8.

65. Lukinavicius, G., K. Umezawa, N. Olivier, A. Honigmann, G. Yang, T. Plass, V. Mueller, L. Reymond, I.R. Correa Jr., Z.G. Luo, C. Schultz, E.A. Lemke, P. Heppenstall, C. Eggeling, S. Manley, and K. Johnsson. 2013. A near-infrared fluorophore for live-cell super-resolution microscopy of cellular proteins. Nat Chem. 5: 132–139.

66. Smith, C.S., N. Joseph, B. Rieger, and K.A. Lidke. 2010. Fast, single-molecule localization that achieves theoretically minimum uncertainty. Nat. Methods. 7: 373–5.

67. Bosch, P.J., J.S. Kanger, and V. Subramaniam. 2014. Classification of dynamical diffusion states in single molecule tracking microscopy. Biophys. J. In press.

68. Panchuk-Voloshina, N., R.P. Haugland, J. Bishop-Stewart, M.K. Bhalgat, P.J. Millard, F. Mao, and W.-Y. Leung. 1999. Alexa Dyes, a Series of New Fluorescent Dyes that Yield Exceptionally Bright, Photostable Conjugates. J. Histochem. Cytochem. 47: 1179–1188.

69. Johnson, L. V, M.L. Walsh, B.J. Bockus, and L.B. Chen. 1981. Monitoring of relative mitochondrial membrane potential in living cells by fluorescence microscopy. J. Cell Biol. 88: 526–35.

70. Stöhr, K. 2008. Fluoreszenzgelöschte Sonder für dianostische und analytische Anwendungen, PhD thesis, Heidelberg University. .

71. Citri, A., and Y. Yarden. 2006. EGF-ERBB signalling: towards the systems level. Nat. Rev. Mol. Cell Biol. 7: 505–16.

72. Wang, Q., G. Villeneuve, and Z. Wang. 2005. Control of epidermal growth factor receptor endocytosis by receptor dimerization, rather than receptor kinase activation. EMBO Rep. 6: 942–8.

73. Hofman, E.G., A.N. Bader, J. Voortman, D.J. Van den Heuvel, S. Sigismund, A.J. Verkleij, H.C. Gerritsen, and P.M.P. Van Bergen En Henegouwen. 2010. Ligand-induced epidermal growth factor receptor (EGFR) oligomerization is kinase-dependent and enhances internalization. J. Biol. Chem. 285: 39481–39489.

74. Lidke, D.S., P. Nagy, R. Heintzmann, D.J. Arndt-Jovin, J.N. Post, H.E. Grecco, E.A. Jares-Erijman, and T.M. Jovin. 2004. Quantum dot ligands provide new insights into erbB/HER receptor-mediated signal transduction. Nat. Biotechnol. 22: 198–203.

75. Altman, R.B., Q. Zheng, Z. Zhou, D.S. Terry, J.D. Warren, and S.C. Blanchard. 2012. Enhanced photostability of cyanine fluorophores across the visible spectrum. Nat. Methods. 9: 428–9.

Figure captions

FIGURE 1   Schematic of the binding of a benzylguanine (BG) substrate to a SNAP-tag fusion protein. The SNAP-tag is fused to a protein of interest. Upon binding, the benzyl group reacts with a cysteine in the active site of SNAP-tag, releasing the guanine group. In this survey the BG was conjugated to fluorescent dyes, but BG can in principle be coupled to any molecule of choice.

FIGURE 2   Fluorescence image of SNAP-tag negative cells incubated with SNAP-tag fluorescent substrates. Incubation of the fluorescent substrates with SNAP-tag negative cells reveals large differences of nonspecific binding to cellular components or the glass surface. Two images showing the staining on SNAP-tag positive cells are included for comparison. The images are recorded in widefield mode on a single molecule sensitive microscope. The field of view was completely confluent with cells. The size of the images is 61x61 μm. The photon intensity scale has not been determined, and varies between images.

FIGURE 3   Quantification of the nonspecific binding of SNAP-tag fluorescent substrates in live cells. The values show the number of mobile and the total number (mobile and immobile) of fluorescent substrates that were nonspecifically bound to cells. The values were determined per field of view area in HeLa, MCF7 and H441 cell lines for each dye showing nonspecific binding on the single molecule level. Some dyes had extremely high levels of nonspecific binding, and since no individual spots could be detected, these were excluded from this graph. Shown are the average number of molecules detected in frames number 20-40 (light grey ▭) and in frames number 120-140 (grey ▬). The field of view is a circular area (1520 μm^2) with a radius of approximately 22 μm. The values were determined in multiple recordings, and the average number is shown here, with the error representing the sample standard deviation.

FIGURE 4   Example of the performed photobleaching analysis on one video recording. A fluorescence image series of SNAP-EGFR labeled with a BG-Dy 549 was recorded. (A) The tracking algorithm finds the molecules in the raw microscope recording, and after exclusion of immobile molecules and very short trajectories, the detected molecules are encircled in the microscopy recording where colors are used to differentiate tracks, see also the online Video 1. (B) The histogram of the number of detected photons per frame of all the found molecules (brightness or spot intensity). The arrow indicates the average of the values, which we defined as the single molecule brightness B. (C) The number of detected molecules per frame $N(i)$ as function of frame number i . In red, a fit of the data using a single exponent exponential decay function according to Eq. 1 to yield the mean photobleaching time τ for each fluorophore. (D) The average brightness of the molecules in one frame does not change over time, evidencing that we indeed looked at single molecules.

FIGURE 5   The expected number of detectable photons per molecule P_{corr} for each SNAP-tag fluorescent substrate. The expected number of photons provides a value for the photostability of a dye conjugate. The values were determined in multiple recordings, and the average number is shown here, with the error representing the sample standard deviation. (A)

The values are corrected for the detection efficiency of the microscope for each dye. (*B*) The values are not corrected for the detection efficiency, and represent the expected number of photons detected in our setup.

FIGURE 6   Comparison of the performance of the SNAP-tag fluorescent substrates for use in single molecule tracking microscopy. The performance is shown in terms of photostability and nonspecific binding. BG-Dy 648 and BG-Dy 649 overlap in the graph. Fluorescent substrates in the lower right corner show little nonspecific attachment to cells, and the most emitted photons per molecule before photobleaching. These substrates are the preferred choice for single molecule tracking microscopy.

FIGURE 7   A TIRF image demonstrating dual color labeling of SNAP-tag receptors at the single molecule level. The labeling was performed on SNAP-EGFR with BG-Dy549 (green) and BG-CF633 (red). The combination of relatively photostable dye conjugates with little nonspecific staining allows multi-color single molecule tracking microscopy. Using this technique receptor homodimers can be directly visualized. See also Video 2.
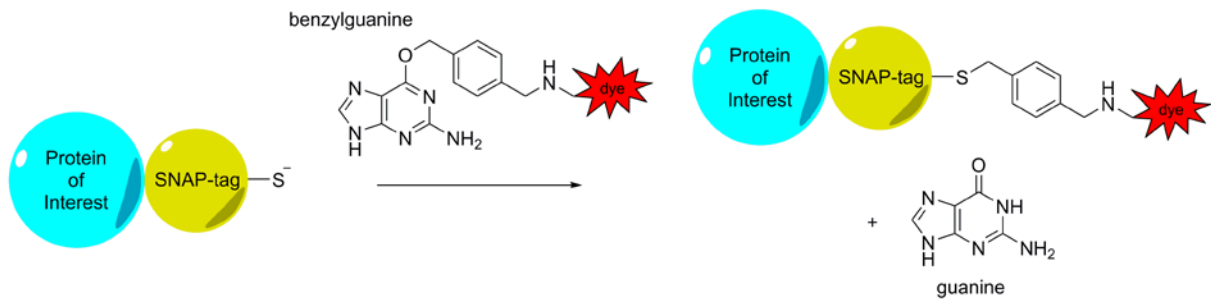
FIGURE 1
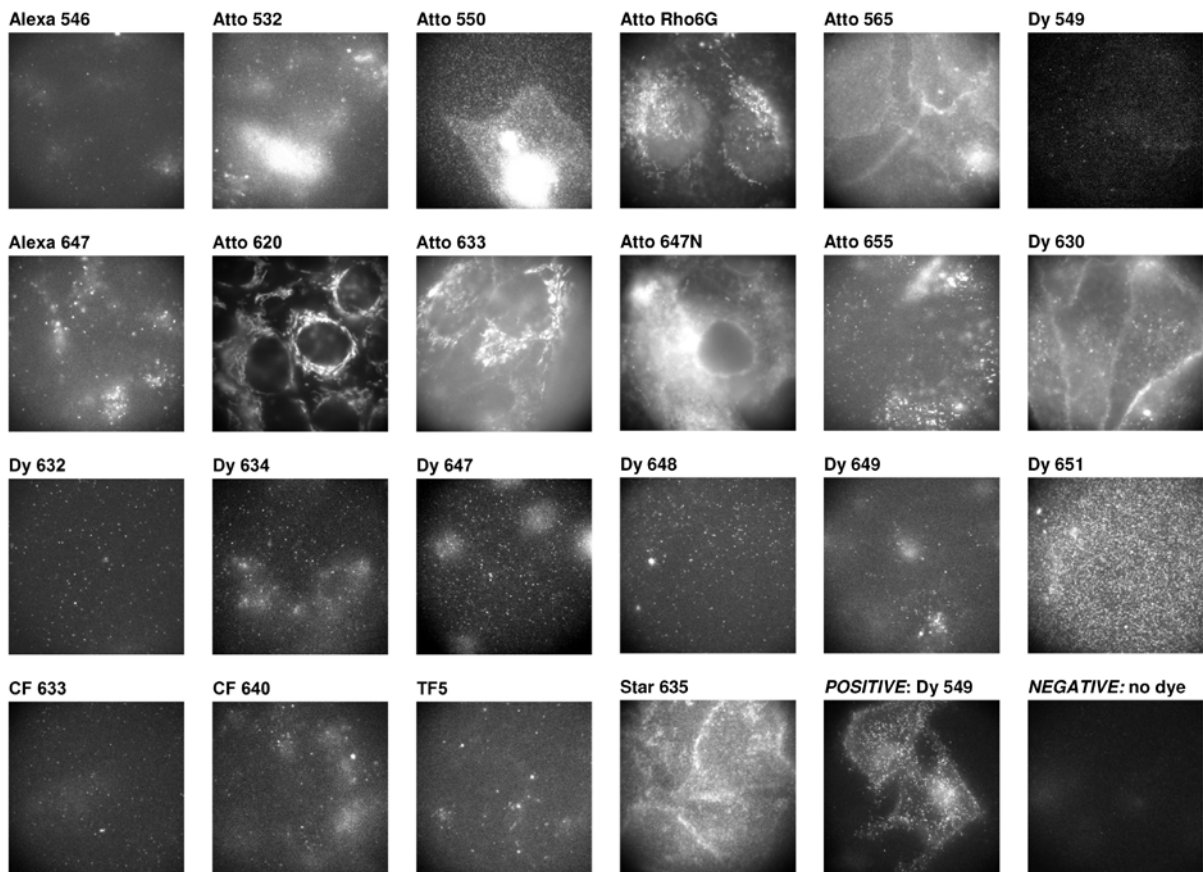
FIGURE 2
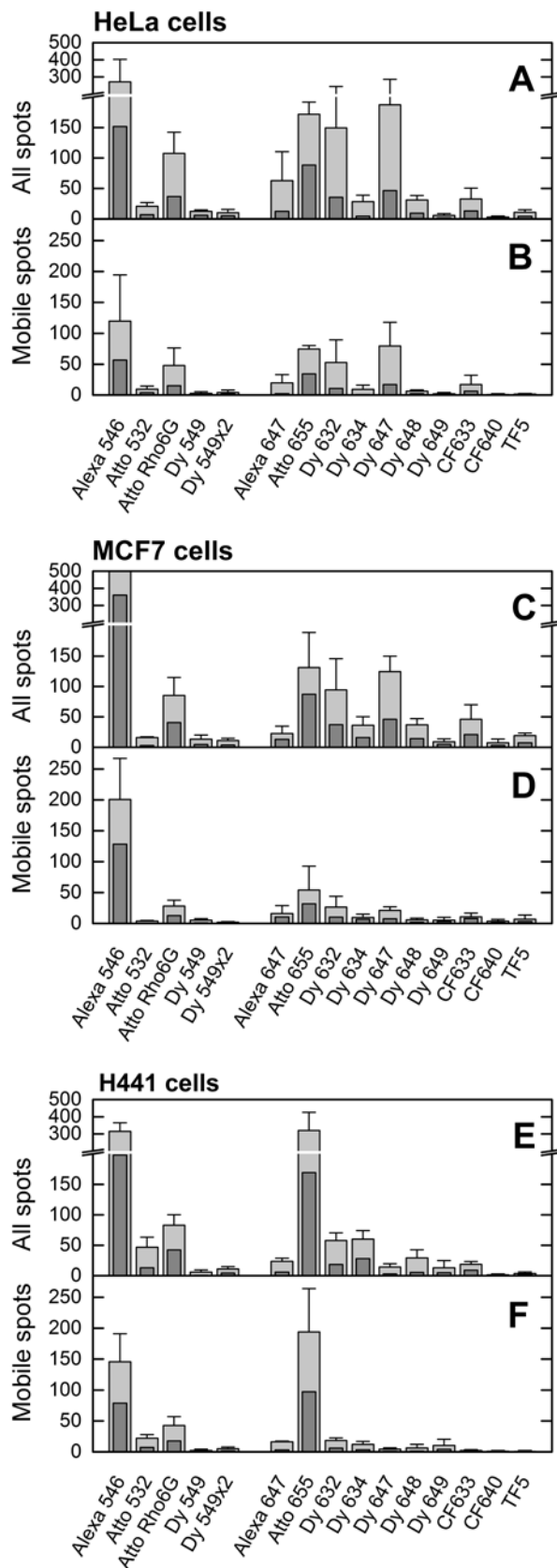
* The following dyes were already excluded due to
high non-specific binding: Atto 550, Atto 565, Atto 620,
Atto 633, Atto 647N, Dy 630, Dy 651, and Star 635

FIGURE 3
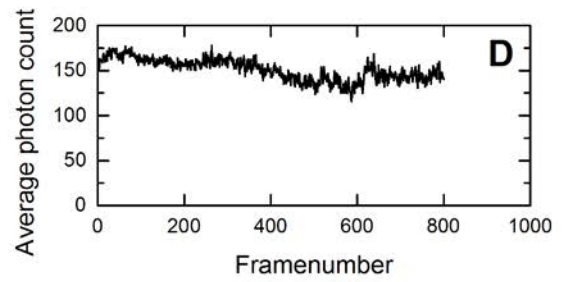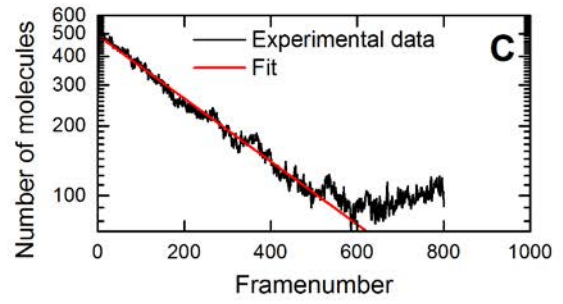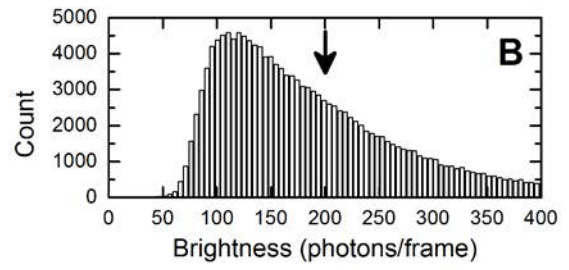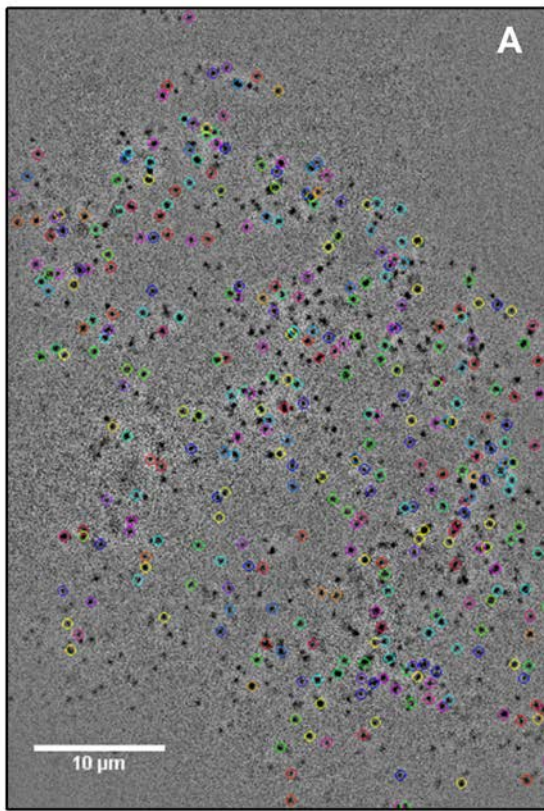
FIGURE 4
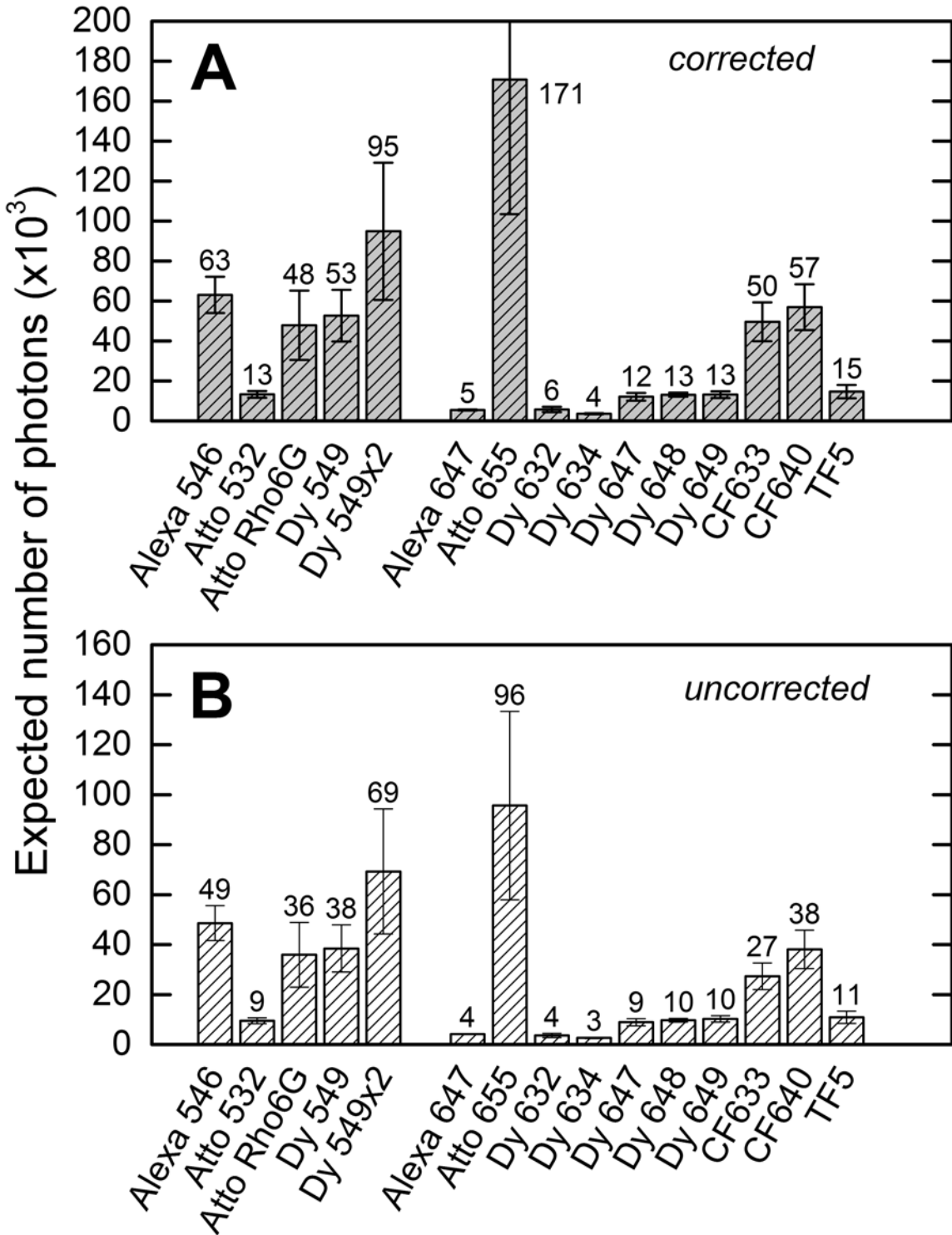
FIGURE 5
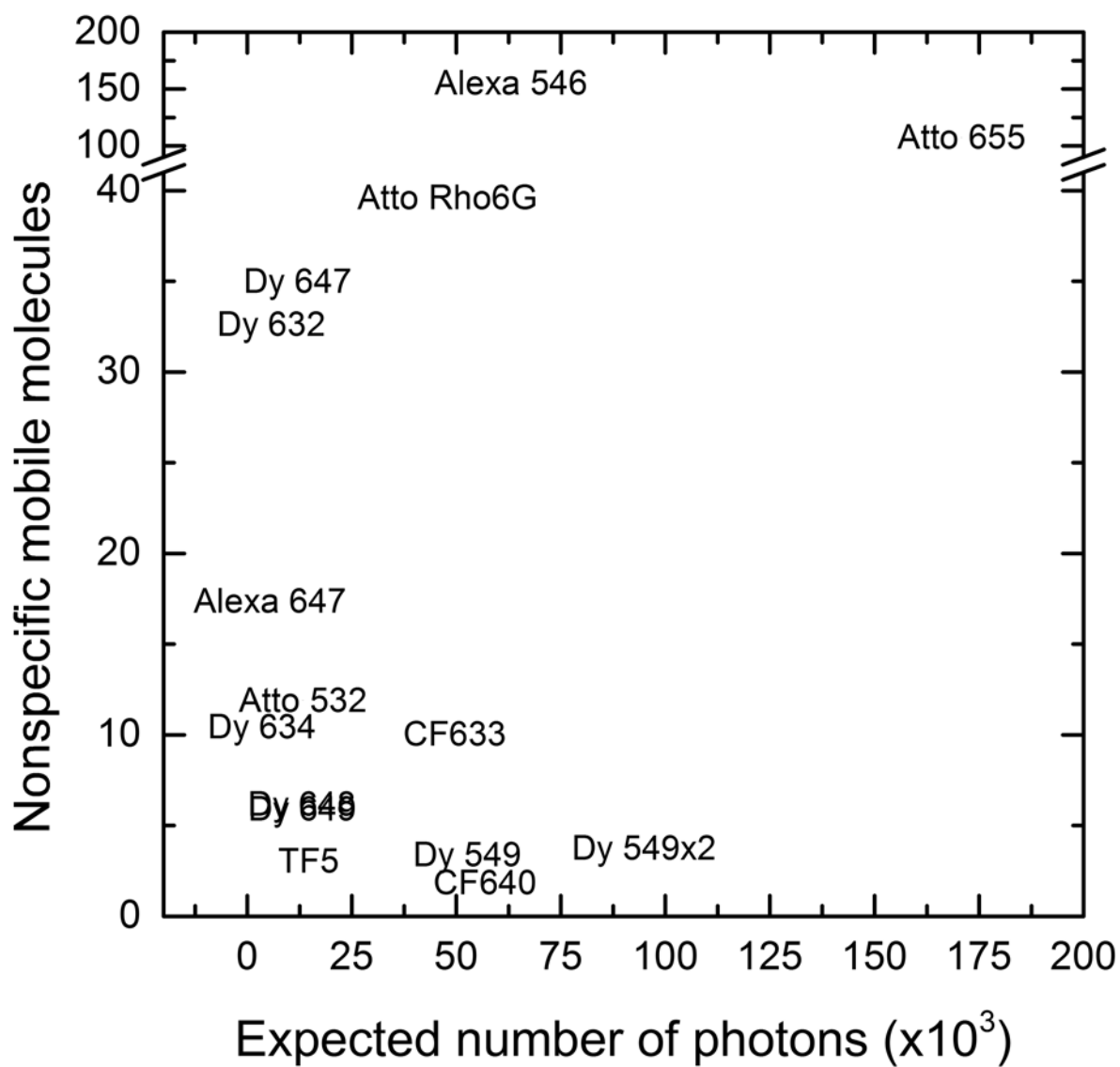
FIGURE 6
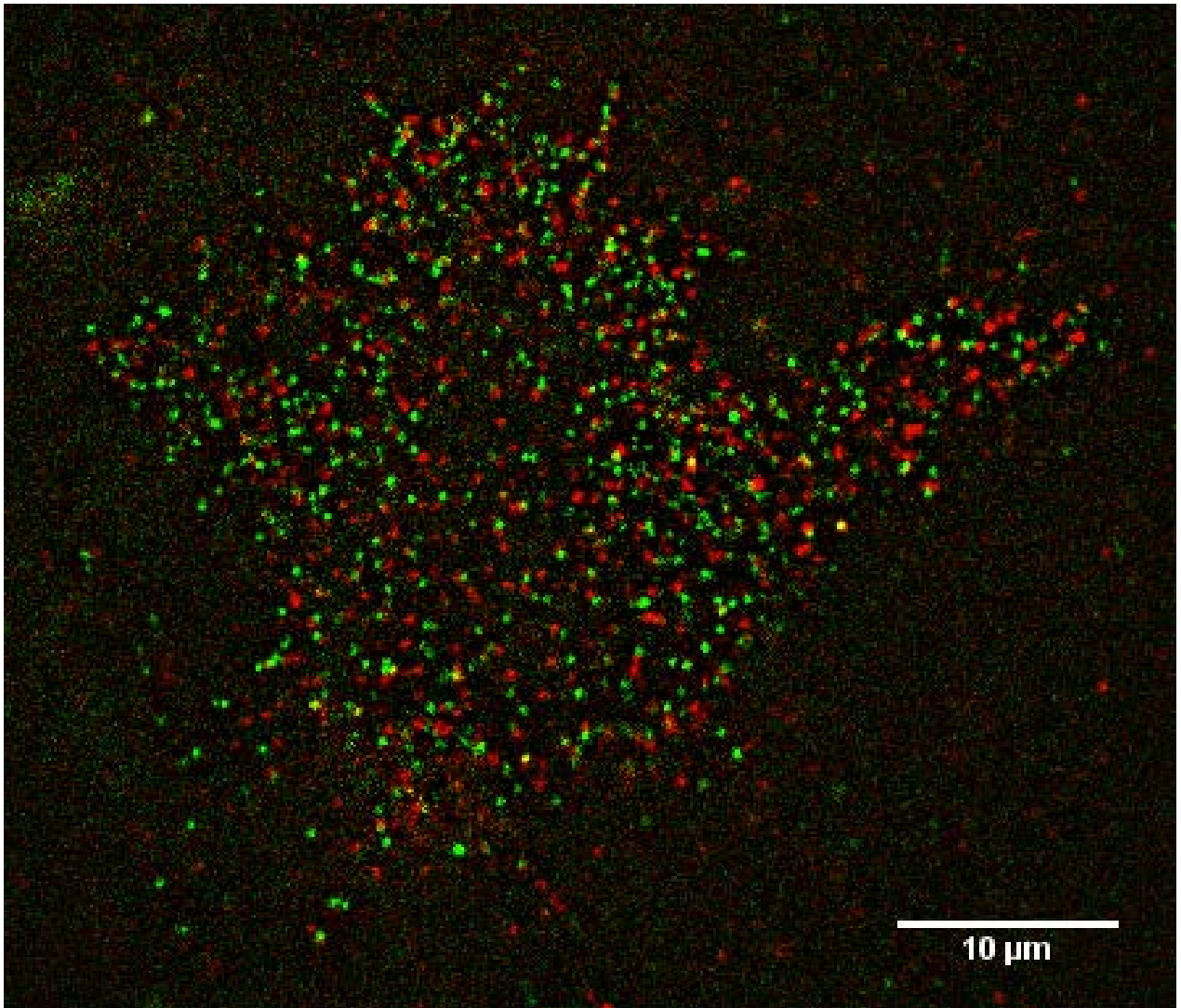
FIGURE 7

Supporting Material for

Evaluation of fluorophores to label SNAP-tag fused proteins for multicolor single molecule tracking microscopy in live cells

Peter J. Bosch[1], Ivan R. Corrêa Jr.[2], Michael H. Sonntag[3], Jenny Ibach[4], Luc Brunsveld[3], Johannes S. Kanger[1], Vinod Subramaniam[1, 5,*]

1. Nanobiophysics, MESA+ Institute for Nanotechnology and MIRA Institute for Biomedical Technology and Technical Medicine, University of Twente, Enschede, The Netherlands
2. New England Biolabs, Ipswich, MA, USA
3. Laboratory of Chemical Biology, Department of Biomedical Engineering, and Institute of Complex Molecular Systems, Eindhoven University of Technology, Eindhoven, The Netherlands
4. Max Planck Institute of Molecular Physiology, Dortmund, Germany
5. Present address: FOM Institute AMOLF, Science Park 104, 1098 XG Amsterdam, The Netherlands

[*]Correspondence: subramaniam@amolf.nl

Contents

1

Supporting figures

FIGURE S1   Calibration of the gain of the two EMCCD cameras performed by the mean-variance method.
The slope of the line in this curve is equal to the inverse gain of the camera. A gain of 49.9 ± 0.1 was found for the camera recording the green-excitable dyes, and a gain of 32.5 ± 0.1 was found for the camera recording the red-excitable dyes.
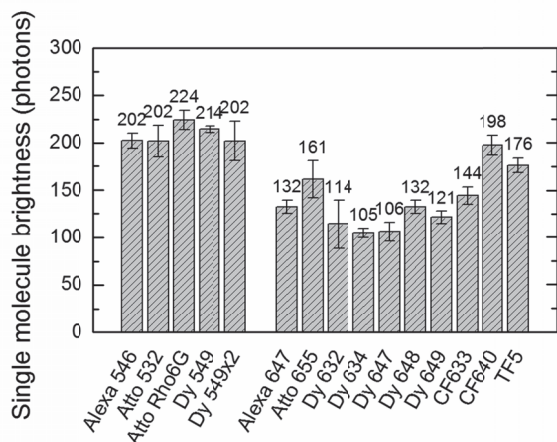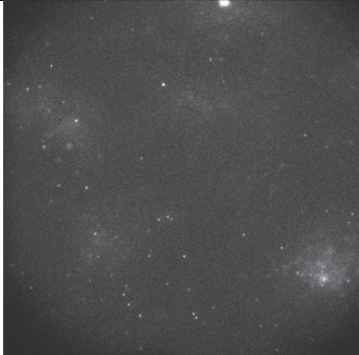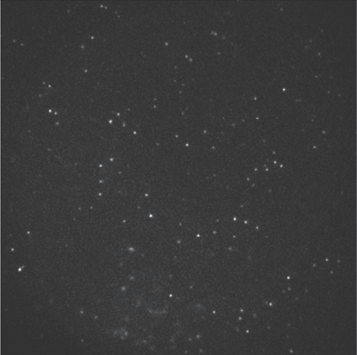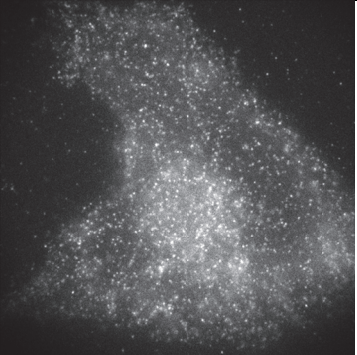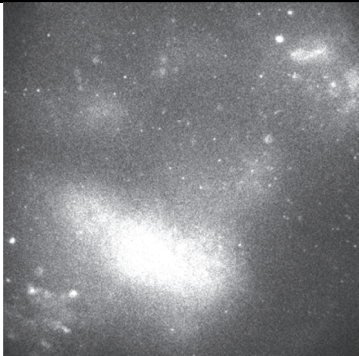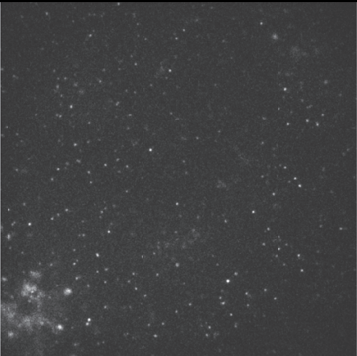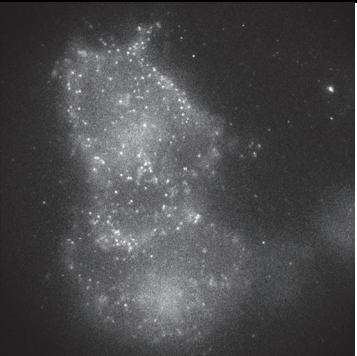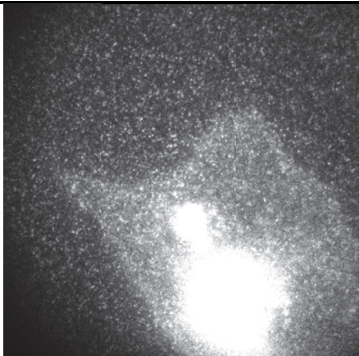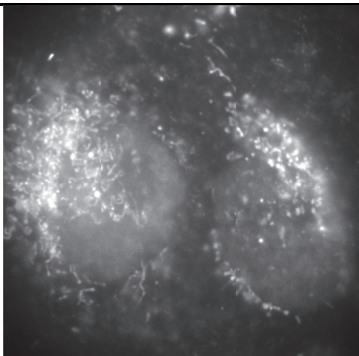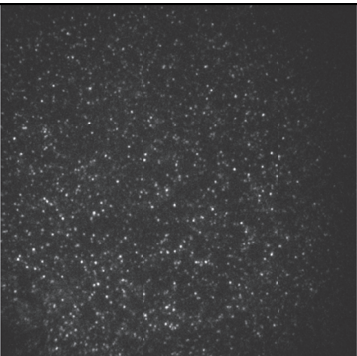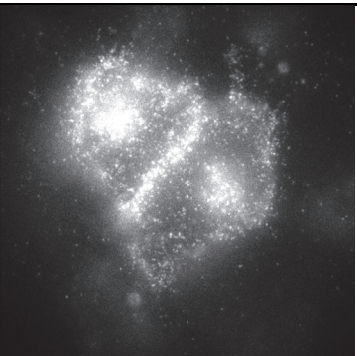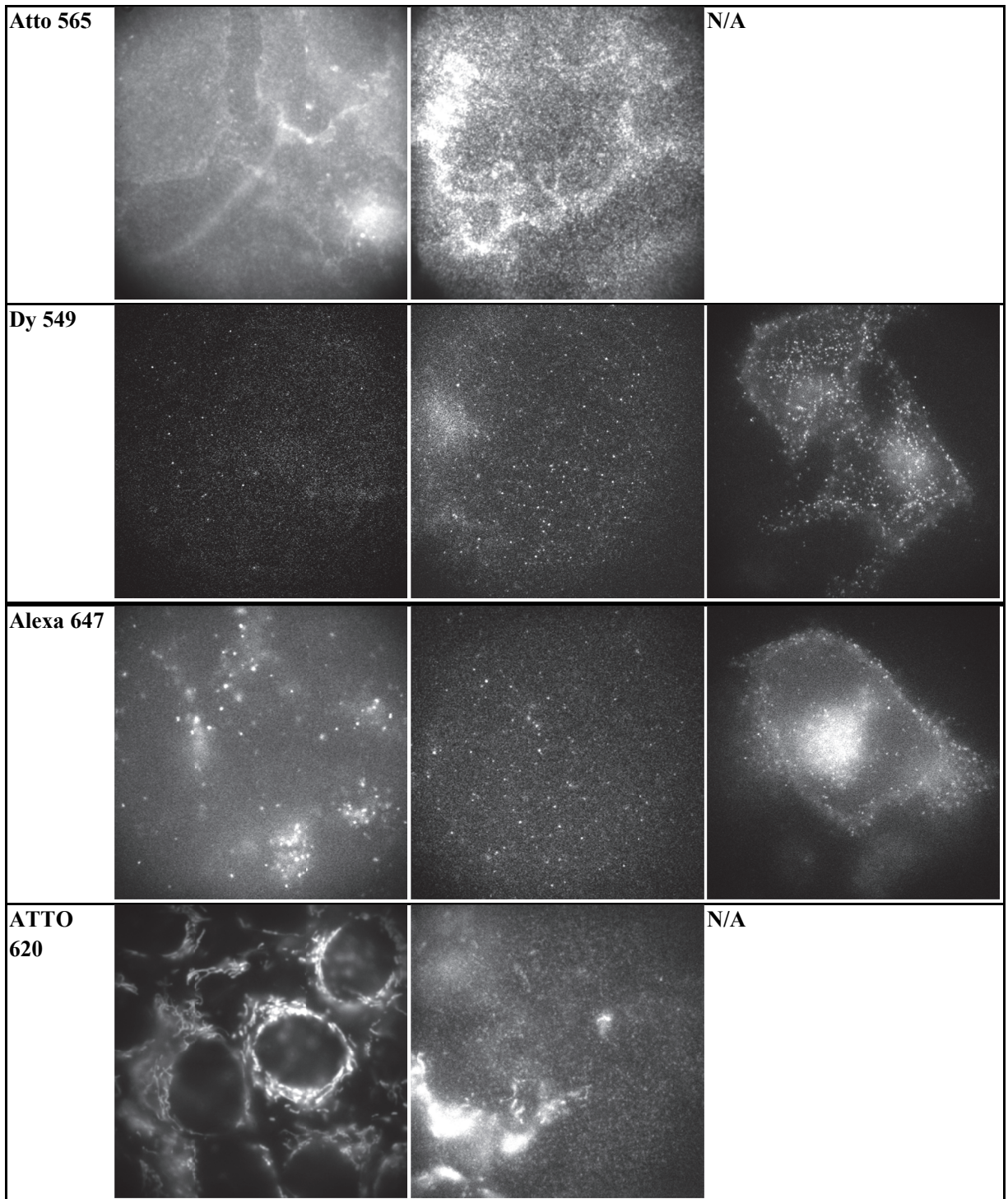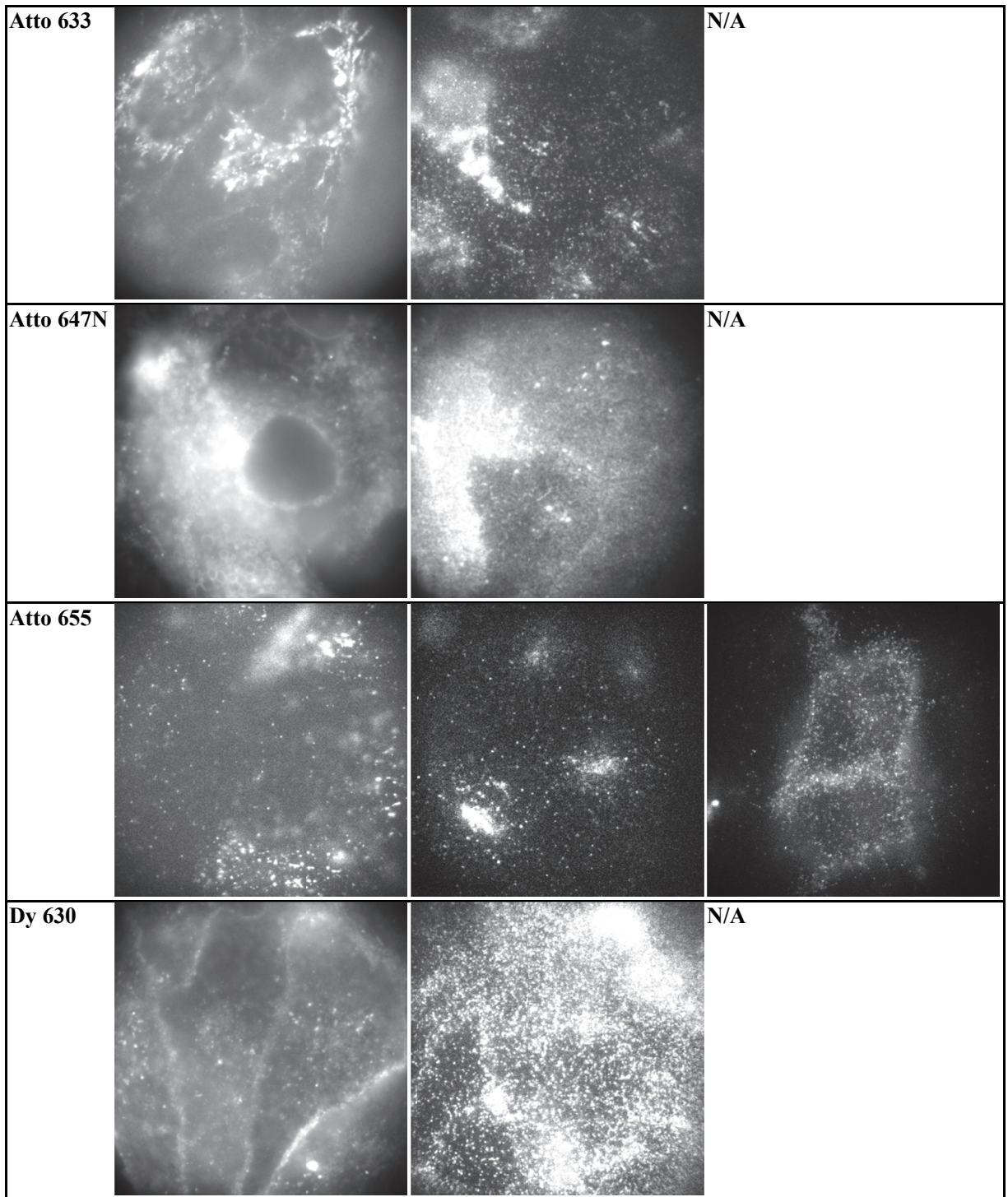

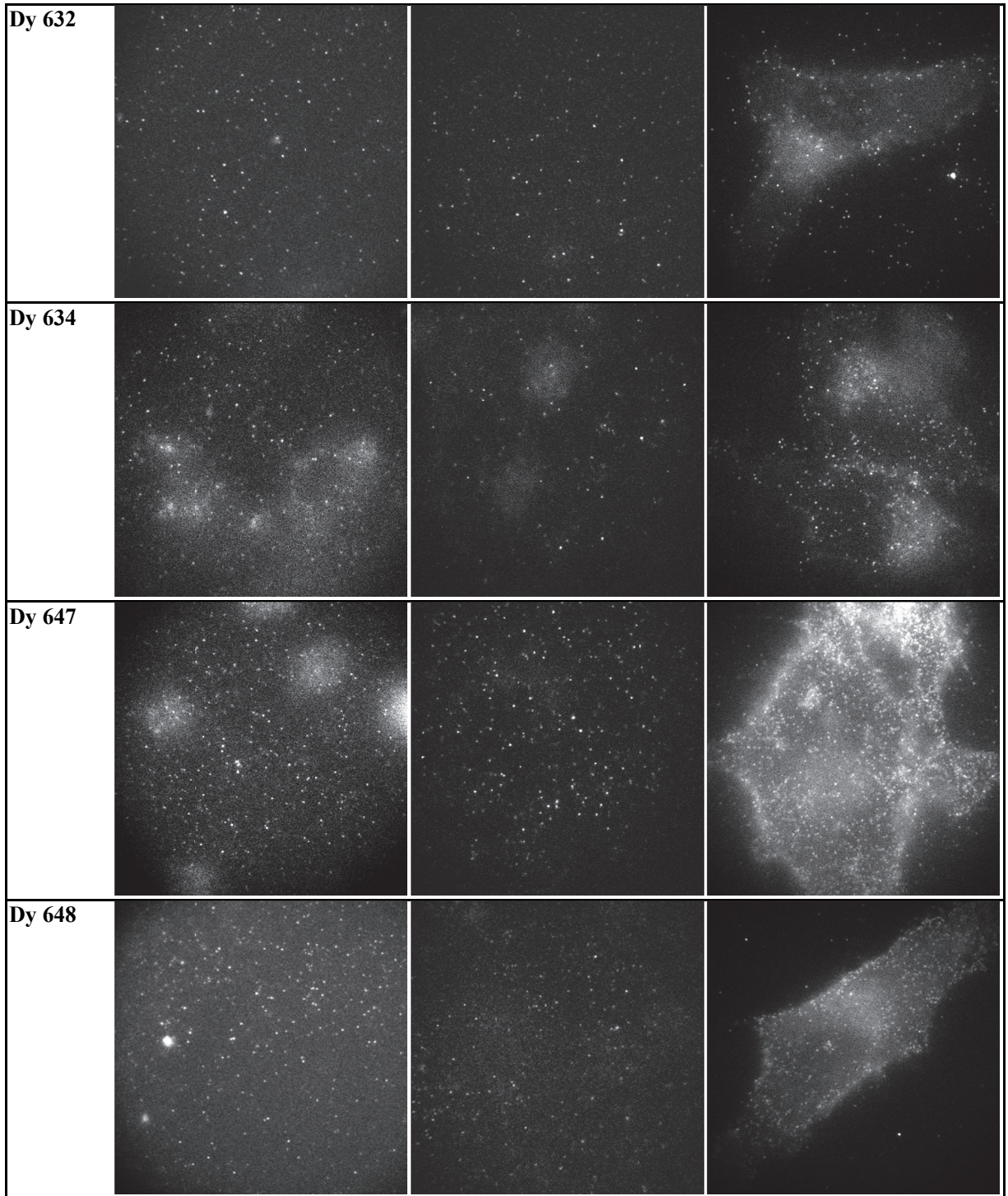**FIGURE S2   The single molecule brightness B per candidate dye.**
Some dyes had extremely high nonspecific level, and since no individual spots could be detected, these are excluded from this graph. Note that the single molecule brightness B was determined without corrections for setup dependent parameters, and therefore differs from the relative intensity of a dye (given in Table S1). The error bars represent the sample standard deviation among multiple videos of the same dye.
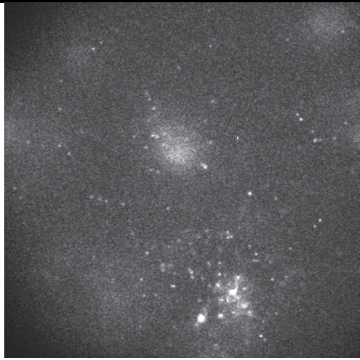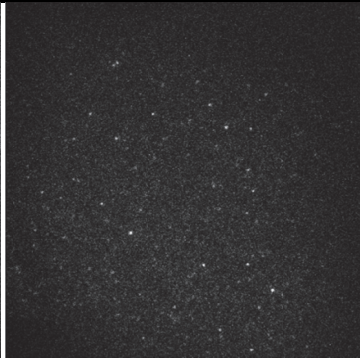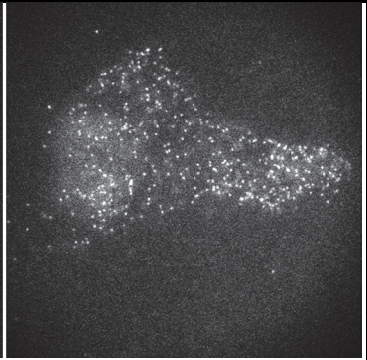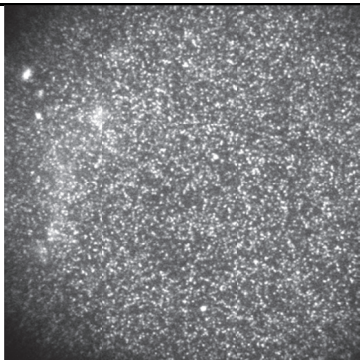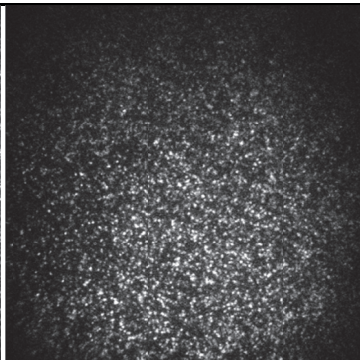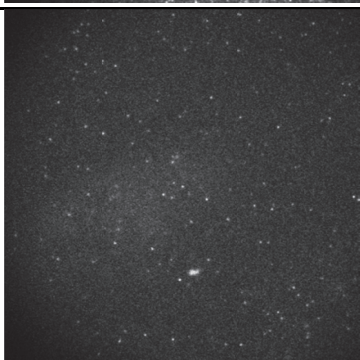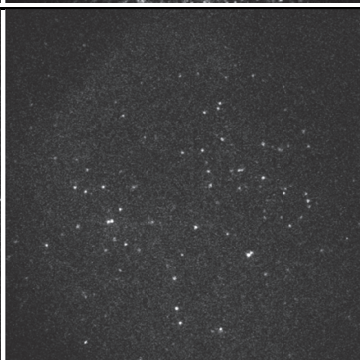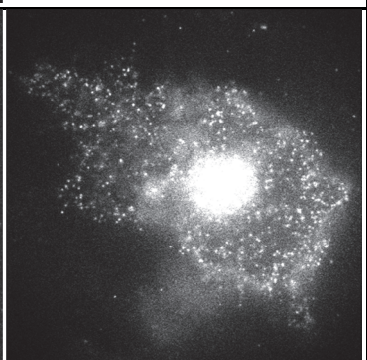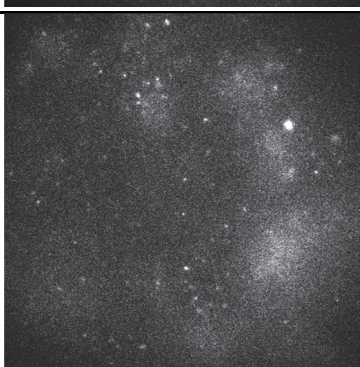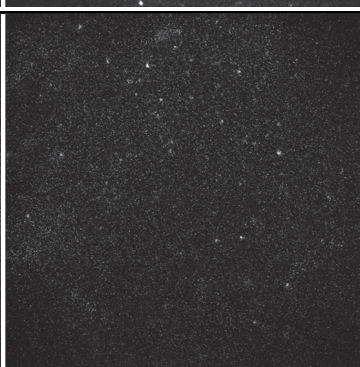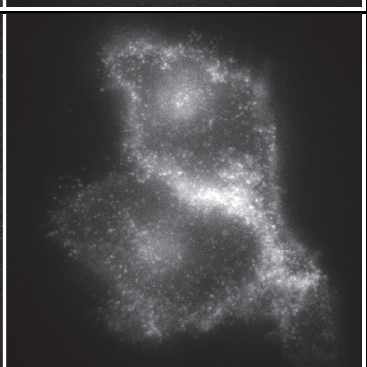
FIGURE S3 *(below)* **Fluorescence images of nonspecific binding of the SNAP substrates.**
Images were recorded in widefield and TIRF illumination setup. The negative images are recordings
of SNAP-tag negative H441 cells. The positive images are recordings of SNAP-tag positive HeLa
cells. The size of the images is 61x61 um, the photon intensity scale has not been determined, and
varies between the shown images. Some images were not acquired (*N/A*) since it was already clear
from nonspecific images that a positive image would not be meaningful.
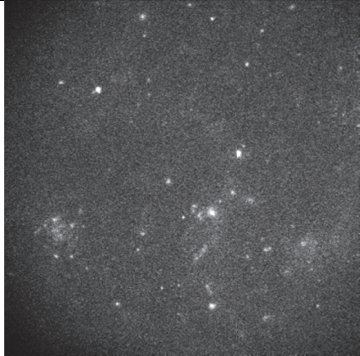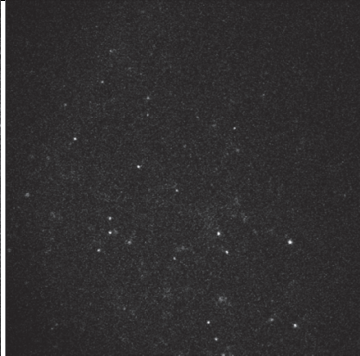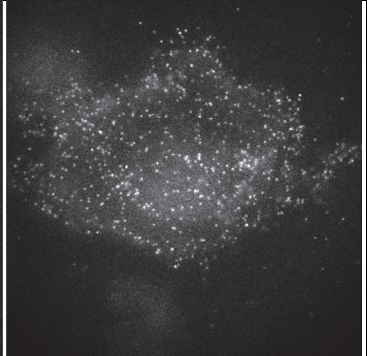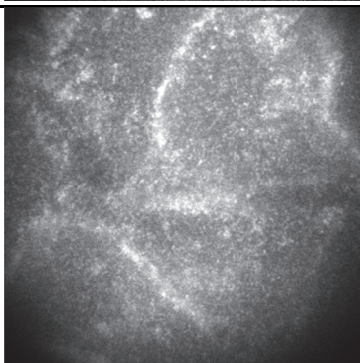
Dye	Negative image in widefield	Negative image in TIRF	Positive image in widefield
Alexa 546			
Atto 532			
Atto 550		N/A	N/A
Atto Rho6G			

Atto 565		N/A
Dy 549		
Alexa 647		
ATTO 620		N/A

Atto 633		**N/A**
Atto 647N		**N/A**
Atto 655		
Dy 630		**N/A**

Dy 632

Dy 634

Dy 647

Dy 648

6

TF5		
Star635	**N/A**	**N/A**

Supporting tables

Table S1:   Efficiency of the excitation and detection of fluorescence in our setup, acquisition time used for microscopy recordings, and resulting relative brightness of the SNAP-tag fluorescent substrates.

BG-dye	Excitation efficiency	Detection efficiency	Acquisition Time (ms)	Relative brightness (%)
Alexa 546	0.32	0.77	15	43
Atto 532	1.00	0.71	10	22
Atto 550	0.40	0.72	n/a [1]	n/a
Atto Rho6G	0.98	0.75	15	16
Dy 549	0.55	0.73	15	28
Dy 549x2	0.55	0.73	15	26
Alexa 647	0.62	0.76	7	58
ATTO 620	0.38	0.46	n/a	n/a
Atto 633	0.87	0.56	n/a	n/a
Atto 647N	0.83	0.63	n/a	n/a
Atto 655	0.62	0.56	19	36
Dy 630	1.00	0.60	n/a	n/a
Dy 632	1.00	0.63	3	88
Dy 634	0.83	0.73	3	84
Dy 647	0.65	0.74	4	80
Dy 648	0.65	0.74	4	100
Dy 649	0.66	0.74	4	86
Dy 651	0.64	0.75	n/a	n/a
CF633	1.00	0.75	8	48
CF640	0.85	0.67	8	63
TF5	0.78	0.74	7	64
Star635	0.99	0.57	n/a	n/a

[1] not acquired, as these substrates showed nonspecific staining above the single molecule level.

9

Table S2:   **Characteristics of the fluorescent substrates in SNAP-tag negative cell lines**

Numbers are rounded to the nearest integer.

Negative control H441 cells

Dye	Raw ph/spot	Total spots frame 20-40			Total spots frame 120-140			Mobile spots fraction frame 20-40
Alexa 546	184	315	±	50	198	±	32	0.46
Atto 532	176	47	±	17	13	±	6	0.47
Atto 550								
Atto Rho6G	189	83	±	17	42	±	7	0.51
Dy 549	231	6	±	3	1	±	1	0.34
Dy 549x2	240	11	±	4	4	±	1	0.46
Alexa 647	118	24	±	5	6	±	3	0.68
ATTO 620								
Atto 633								
Atto 647N								
Atto 655	147	320	±	106	170	±	52	0.61
Dy 630								
Dy 632	73	58	±	13	19	±	1	0.32
Dy 634	84	60	±	14	28	±	6	0.20
Dy 647	128	14	±	5	3	±	2	0.30
Dy 648	147	29	±	13	5	±	3	0.21
Dy 649	137	13	±	12	5	±	4	0.80
Dy 651								
CF633	145	19	±	5	9	±	2	0.12
CF640	210	1	±	2	0	±	0	0.75
TF5	179	4	±	2	2	±	1	0.19

Negative control HeLa cells

Dye	Raw ph/spot	Total spots frame 20-40			Total spots frame 120-140			Mobile spots fraction frame 20-40
Alexa 546	191	272	±	131	151	±	112	0.44
Atto 532	178	21	±	6	7	±	2	0.47
Atto 550								
Atto Rho6G	208	108	±	35	37	±	13	0.45
Dy 549	197	12	±	3	6	±	2	0.23
Dy 549x2	189	10	±	5	5	±	3	0.44
Alexa 647	61	63	±	47	12	±	8	0.32
ATTO 620								
Atto 633								
Atto 647N								
Atto 655	147	172	±	20	88	±	11	0.44
Dy 630								
Dy 632	63	149	±	95	35	±	23	0.35
Dy 634	75	28	±	11	4	±	2	0.34
Dy 647	98	187	±	99	47	±	16	0.42
Dy 648	230	31	±	7	9	±	2	0.21
Dy 649	92	6	±	3	2	±	1	0.37
Dy 651								
CF633	141	32	±	18	13	±	6	0.53
CF640	175	3	±	2	1	±	0	0.32
TF5	230	11	±	4	4	±	2	0.15

Negative control MCF7 cells

Dye	Raw ph/spot	Total spots frame 20-40			Total spots frame 120-140			Mobile spots fraction frame 20-40
Alexa 546	206	512	±	101	361	±	97	0.39
Atto 532	169	16	±	1	3	±	0	0.24
Atto 550								
Atto Rho6G	215	85	±	30	41	±	11	0.33
Dy 549	252	13	±	7	5	±	2	0.39
Dy 549x2	200	11	±	4	4	±	2	0.17
Alexa 647	116	23	±	12	13	±	11	0.71
ATTO 620								
Atto 633								
Atto 647N								
Atto 655	149	131	±	58	87	±	36	0.41
Dy 630								
Dy 632	84	94	±	51	37	±	17	0.28
Dy 634	94	36	±	14	16	±	4	0.27
Dy 647	124	124	±	26	46	±	8	0.17
Dy 648	139	37	±	10	14	±	5	0.16
Dy 649	96	9	±	5	5	±	5	0.57
Dy 651								
CF633	159	46	±	24	21	±	11	0.23
CF640	220	8	±	6	3	±	3	0.47
TF5	226	19	±	4	7	±	1	0.35

Supporting methods

General Procedure for the Synthesis of SNAP-tag substrates

For BG-Dy 651, BG-CF633, BG-CF640R and BG-Star 635, reactions were performed at $1 - 2$ µmol scale using 1.0 equiv of BG-NH$_2$ in anhydrous *N,N*-dimethylformamide (DMF) in the presence of triethylamine (2.0 equiv), and the corresponding fluorophore N-hydroxysuccinimidyl ester (1.0 equiv), at room temperature. For BG-Atto Rho6G, BG-Dy 630, BG-Dy 634, and BG-Dy 648, reactions were performed at 0.1 µmol scale using 1.0 equiv of BG-NH$_2$, 1% triethylamine, and $3.0 - 4.0$ equiv of the fluorophore N-hydroxysuccinimidyl ester, at 30°C. BG-Dy 549-549 (BG-549-549) was synthesized by reacting the bifunctional building block BG-Lys(Dde)-Fmoc (76) with a 2% solution of hydrazine in DMF (0.5 mL), followed by solvent removal under high vacuum overnight, and treatment with 2.2 equiv of triethylamine and 2.2 equiv of Dy549 N-hydroxysuccinimidyl ester at room temperature. All coupling reactions were carried out for 12 h. Reaction completion was monitored by HPLC. Reaction mixtures were concentrated and purified by reversed-phase HPLC. Each substrate was analyzed by mass spectrometry and UV absorption. Isolated yields are given in parentheses when determined and are not optimized. BG-CF633 (54%): ESI-MS *m/z* 1074.4 $[M+H]^+$, λ_{max}=630 nm; BG-CF640R (80%): ESI-MS *m/z* 1083.3 $[M-H]^-$, λ_{max}=642 nm; BG-Star635 (30%): ESI-MS *m/z* 1148.3 $[M+H]^+$, λ_{max}=631 nm; BG-651 (35%): ESI-MS *m/z* 1019.3 $[M+H]^+$, λ_{max}=656 nm; BG-AttoRho6G: ESI-MS *m/z* 766.6 $[M+H]^+$, λ_{max}=535 nm; BG-Dy630: ESI-MS *m/z* 887.6 $[M+H]^+$, λ_{max}=631 nm, BG-Dy634: ESI-MS *m/z* 1155.5 $[M+H]^+$, λ_{max}=631 nm, BG-Dy648: ESI-MS *m/z* 989.5 $[M+H]^+$, λ_{max}=650 nm; BG-Dy 549x2 (61%): ESI-MS *m/z* 998.8 $[M-2H]^{2-}$, λ_{max}=557 nm.

SNAP-EGFR construct

SNAP-EGFR was cloned by replacing the EGFP in EGFP-EGFR (originated from pEGFP-N1 (New England Biolabs (NEB)) with NheI/NotI restriction sites and the 24 amino acid signaling sequence of EGFR in front of EGFP) by a SNAP-tag. The sequence for SNAP was amplified by PCR from pSNAP-tag(m) (NEB) with the primers SNAP_AgeI_F (GCG ACC GGT AAT GGA CAA AGA CTG CGA AAT G) and SNAP_XhoI_R (CTC CTC GAG CAC CCA GCC CAG GCA), digested with AgeI (NEB) and XhoI (NEB) and cloned into the AgeI/XhoI restriction sites of the digested EGFP-EGFR plasmid.

Microscope hardware

Measurements were performed on an inverted microscope with an Olympus PlanApo 100x/1,45 Oil TIRF objective. For the excitation we used a 532 nm 400 mW solid state laser from Pegasus Shanghai Optical Systems (Pegasus Lasersysteme, Wallenhorst, Germany), and a 637 nm 300 mW diode laser from Changchun New Industries Optoelectronics (Laser 2000, Vinkeveen, The Netherlands). The infrared light produced by the lasers was not sufficiently suppressed; we therefore filtered the green laser light with an FF01-543/22 (SemRock, Rochester, NY) filter and the red laser light with a D644/10m (Chroma, Olching, Germany) bandpass filter. The two laser beams were combined with a 610 nm longpass mirror. An achromatic quarter wave plate (VM-TIM Optomechanische Werke, Jena, Germany) was used to obtain circularly polarized excitation light. An FF494/540/650-Di01 (SemRock) dichroic mirror separated the excitation light from the emission light. The optical path and filters reduced the power of the laser light reaching the objective. For the green laser 88 mW was measured after the objective, and for the red laser 47 mW was measured after the objective. The excitation field of view had an approximate diameter of 60 µm, which resulted in an estimated 3.1 and 1.7 kW/cm^2 for the green and red excitation intensity respectively. The emission light was filtered with an NF03-532/1064E (SemRock) and an NF02-633S (SemRock) notch filter, and then split with an FF640-FDi01 (SemRock) imaging flatness quality dichroic mirror. The emission light from the green

excitation dyes was passed through a FF01-580/60 (SemRock) bandpass filter, and the light from the red excitation dyes through a HQ680/60m (Chroma) bandpass filter. The images were acquired using two Andor iXon EM+ DU-897 back illuminated EMCCD cameras. Using a calibration sample with grid lines separated at known distances, we determined that the pixel size was 119 ± 2 nm (the magnification was 134x). The sample was only illuminated during the acquisition time by utilizing the TTL output of the camera and TTL input of the lasers. Samples were heated to 35-37°C on the microscope with a stage heating plate and an objective ring heater.

Settings file for SPT tracking software

Dat.PixelSize = .119;
Dat.TimeStep = 0.04468;|
Dat.ch_bin = [1];
Params.verbose = 1;
Params.frames = [];

Params.psf = [0.84034 0.84034];
Params.imMask = [];
Params.wvMask = [];
Params.CCDGain = 32.5;
Params.CCDOffset = 0;
Params.Intensity = 3.70;
Params.FitBoxSize = [7];
Params.Iterations = 10;
Params.MaxCudaFits = 30000;
Params.MinCRLBSigma = 0.5;
Params.MinPValue = 0.01;
Params.MinPhotons = [10];
Params.ConnectParams.costMatF2Fparams = costMatFrame2FrameSetOptions;
Params.ConnectParams.costMatGCparams = costMatCloseGapsSetOptions;
%%% set parameters for frame 2 frame connections %%%
Params.ConnectParams.costMatF2Fparams.funcName = 'costMatFrame2FrameDensity';
Params.ConnectParams.costMatF2Fparams.density = [];
Params.ConnectParams.costMatF2Fparams.D = [0.06*Dat.TimeStep/Dat.PixelSize^2
0.06*Dat.TimeStep/Dat.PixelSize^2];
Params.ConnectParams.costMatF2Fparams.maxSearchDist = [4 4];
Params.ConnectParams.costMatF2Fparams.kon = 0.1;
Params.ConnectParams.costMatF2Fparams.koff = 0.0001;
Params.ConnectParams.costMatF2Fparams.maxWvSearchDist = [];
Params.ConnectParams.costMatF2Fparams.wvJump = [];
%%% set parameters for gap closing %%%
Params.ConnectParams.costMatGCparams.timeWindow = 10;
Params.ConnectParams.costMatGCparams.funcName = 'costMatCloseGapsDensityM';
Params.ConnectParams.costMatGCparams.density = [];
Params.ConnectParams.costMatGCparams.D = [0.01 0.01];
Params.ConnectParams.costMatGCparams.maxSearchDistPerFrame = [3 3];
Params.ConnectParams.costMatGCparams.maxSearchDist = [10 10];
Params.ConnectParams.costMatGCparams.minTrackLen = 2;
Params.ConnectParams.costMatGCparams.kon = 0.1;
Params.ConnectParams.costMatGCparams.koff = 0.0001;
Params.ConnectParams.costMatGCparams.maxWvSearchDist = [];
Params.ConnectParams.costMatGCparams.wvJump = [];
Params.TrackFunction = 'obj.makeTrack';